

柴北缘欧龙布鲁克地块中元古代晚期麻粒岩相变质作用

——来自石榴夕线堇青石片麻岩的岩石学、相平衡模拟和 U-Pb 年代学的制约

毛小红¹, 路增龙², 张建新¹, 郭祺^{1,3}, 武亚威^{1,3}

(1. 中国地质科学院地质研究所 自然资源部深地动力学重点实验室, 北京 100037; 2. 中色紫金地质勘查(北京)有限责任公司, 北京 100012; 3. 北京大学 地球与空间科学学院, 北京 100871)

摘要: 在欧龙布鲁克地块乌兰北部地区察汗河岩群中识别出麻粒岩相石榴夕线堇青石片麻岩, 其矿物组合为石榴子石、夕线石、堇青石、黑云母、斜长石、钛铁矿和少量钾长石等。岩相学观察显示, M1 阶段矿物组合有斜长石±钾长石+石榴子石+夕线石+石英, M2 阶段矿物组合有斜长石±钾长石+石榴子石+夕线石+石英+钛铁矿+黑云母, M3 阶段矿物组合有堇青石+黑云母+钛铁矿+石英+石榴子石+斜长石±钾长石。相平衡模拟计算结果显示, 该岩石的峰期温压条件为 $p=0.92\sim1.08$ GPa, 峰期温度 $t>790^{\circ}\text{C}$, 峰期之后经历升温降压的 $p-T$ 演化轨迹。锆石和独居石 LA-ICP-MS U-Pb 年代学研究获得的变质年龄分别为 1133 ± 14 Ma 和 1125 ± 37 Ma, $1133\sim1125$ Ma 应代表了该期麻粒岩相变质作用的时代。结合区域地质资料和已有的研究成果, 我们认为乌兰北部察汗河岩群的石榴夕线堇青石片麻岩可能形成于大洋俯冲作用下的弧或弧后构造环境, 乌兰北部的岩浆-变质杂岩带经历了从中元古代晚期-新元古代早期俯冲增生到碰撞造山的演化过程, 是全球 Rodinia 超大陆汇聚过程的响应。

关键词: 欧龙布鲁克地块; 石榴夕线堇青石片麻岩; 麻粒岩相; Rodinia 超大陆; 相平衡模拟

中图分类号: P588.34⁺5; P597⁺.3 文献标识码: A 文章编号: 1000-6524(2024)02-0219-19

Late Mesoproterozoic granulite-facies metamorphism in the Oulongbuluke block of the North Qaidam Mountains: Constraints from petrology, phase equilibrium modeling and U-Pb dating of garnet-sillimanite-cordierite gneisses

MAO Xiao-hong¹, LU Zeng-long², ZHANG Jian-xin¹, GUO Qi^{1,3} and WU Ya-wei^{1,3}

(1. Key Laboratory of Deep-Earth Dynamics of Ministry of Natural Resources, Institute of Geology, Chinese Academy of Geological Sciences, Beijing 100037, China; 2. Sino-Zijin Resources Ltd., Beijing 100012, China; 3. School of Earth and Space Sciences, Peking University, Beijing 100871, China)

Abstract: The garnet-sillimanite-cordierite gneiss, which has been identified from the Chahanhe Group in the northern region of the Oulongbuluke block, consists of garnet, sillimanite, cordierite, biotite, plagioclase, ilmenite, and a

收稿日期: 2023-12-05; 接受日期: 2024-01-28; 编辑: 郝艳丽

基金项目: 国家自然科学基金项目(42102246, 42202058); 中国地质科学院基本科研业务费项目(JKYZD202310); 中国地质科学院地质研究所基本科研业务费项目(J2319)

作者简介: 毛小红(1983-), 女, 博士, 助理研究员, 构造地质学专业, E-mail: mxhcj40241055@163.com; 通讯作者: 张建新(1966-), 男, 博士, 研究员, 长期从事造山带变质变形作用研究, E-mail: zjx66@yeah.net。

small amount of K-feldspar. Petrographic observation shows that three stages (M1, M2 and M3) of mineral assemblage can be recognized. They are M1: Pl±Kfs+Grt+Sill+Qz, M2: Pl±Kfs+Grt+Sill+Qz+Ilm+Bt, and M3: Crd+ Bt+Ilm+Qz+Grt+Pl±Kfs. Phase equilibrium modelling shows that the peak p - T conditions of the garnet-sillimanite-cordierite rock are $p = 0.92 \sim 1.08$ GPa and $t > 790^\circ\text{C}$, and experienced a heating decompression during exhumation. The metamorphic ages acquired from zircon and monazite U-Pb dating by LA-ICP-MS are 1133 ± 14 Ma and 1125 ± 37 Ma, respectively, which represent the timing of granulite-facies metamorphism. Combining regional geology with our data, we suggested that the garnet-sillimanite-cordierite rock in the Chahanhe Group formed in an arc or back-arc system related to oceanic subduction. The magmatic-metamorphic complex belt in the northern region of the Oulongbuluke block underwent an evolutionary process from subduction-accretion to collision orogeny during late Mesoproterozoic to early Neoproterozoic, which is a response to the convergence process of Rodinia supercontinent.

Key words: Oulongbuluke block; garnet-sillimanite-cordierite gneiss; granulite-facies; Rodinia supercontinent; phase equilibrium modelling

Fund support: National Natural Science Foundation of China (42102246, 42202058); Basic Scientific Research Fund of Chinese Academy of Geological Sciences (JKYZD202310); Basic Scientific Research Fund of Institute of Geology, Chinese Academy of Geological Sciences (J2319)

柴达木盆地北缘的欧龙布鲁克地块(又称“全吉地块”)位于青藏高原的东北部,中央造山带的中西段,南部以柴北缘高压-超高压变质带为界与柴达木地块相隔,北以宗务隆断裂(构造带)与南祁连俯冲增生杂岩带和祁连地块相隔,其西端被阿尔金断裂所截,往东延至鄂拉山与秦岭造山带交会,东西延伸

800余千米(图1)。已有研究显示,欧龙布鲁克地块具有克拉通性质的二元结构,其基底由深变质的古元古代深成侵入体(德令哈杂岩)和变质表壳岩(达肯肯达坂群)组成,其上不整合覆盖有中元古代以来的未(浅)变质的沉积盖层(陆松年等,2002;陈能松等,2007;张建新等,2021)。然而,近年的研究显示,

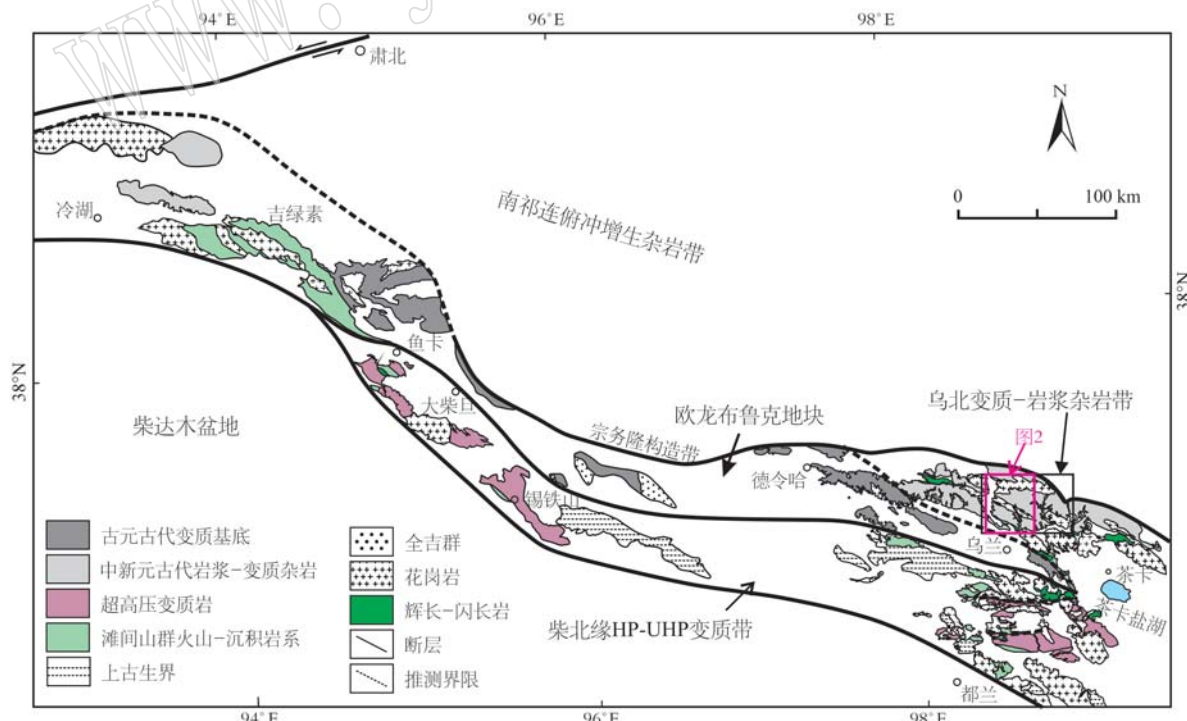


图 1 欧龙布鲁克地块及其邻区地质图[据路增龙等(2020 修改)]

Fig. 1 Geological map of Oulongbuluke block and adjacent area(modified after Lu Zenglong et al., 2020)

在原归为欧龙布鲁克地块的乌兰北部地区,其所谓“达肯达坂群”的深变质岩的原岩时代主要为中元古代,并伴有中新元古代的岩浆侵入体。一些学者把乌北地区主要由中元古代表壳岩和中-新侵入体组成的变质-岩浆杂岩从欧龙布鲁克地块中解体出来,称之为“乌北地块”(Wang *et al.*, 2016)。近年来,我们及其他学者发现这些深变质岩石普遍经历了早古生代的低压-高温变质作用,并伴随早古生代弧岩浆岩的侵位(李秀财等, 2015a; Lu *et al.*, 2018; Wang *et al.*, 2018; Li *et al.*, 2019),我们又称之为乌兰北早古生代弧(弧后)变质-岩浆杂岩带(Lu *et al.*, 2018; 张建新等, 2021)。因此,查明乌兰北部

地区高级变质岩-岩浆杂岩的组成和年代格架,解析其经历的多期构造热历史,揭示欧龙布鲁克地块的性质,对重新认识中央造山带中的前寒武纪地块的起源、区域地层划分及区域构造格局的重建乃至超大陆的演化具有重要的启示意义。

乌兰北部变质-岩浆杂岩带西起老虎口以西,东到茶卡以北,呈 NWW-SEE 展布,在乌兰北部察汗河村-哈里哈图一带,主要分布有中新元古代的副变质岩系(察汗河岩群)、中新元古代多期次的变质长英质侵入岩(包括约 1.5 Ga、约 1.1 Ga 及约 0.9 Ga 的正片麻岩)、古生代和早中生代岩浆岩及少量滩间山群浅变质火山-沉积岩(图2)。本文以察汗河岩群

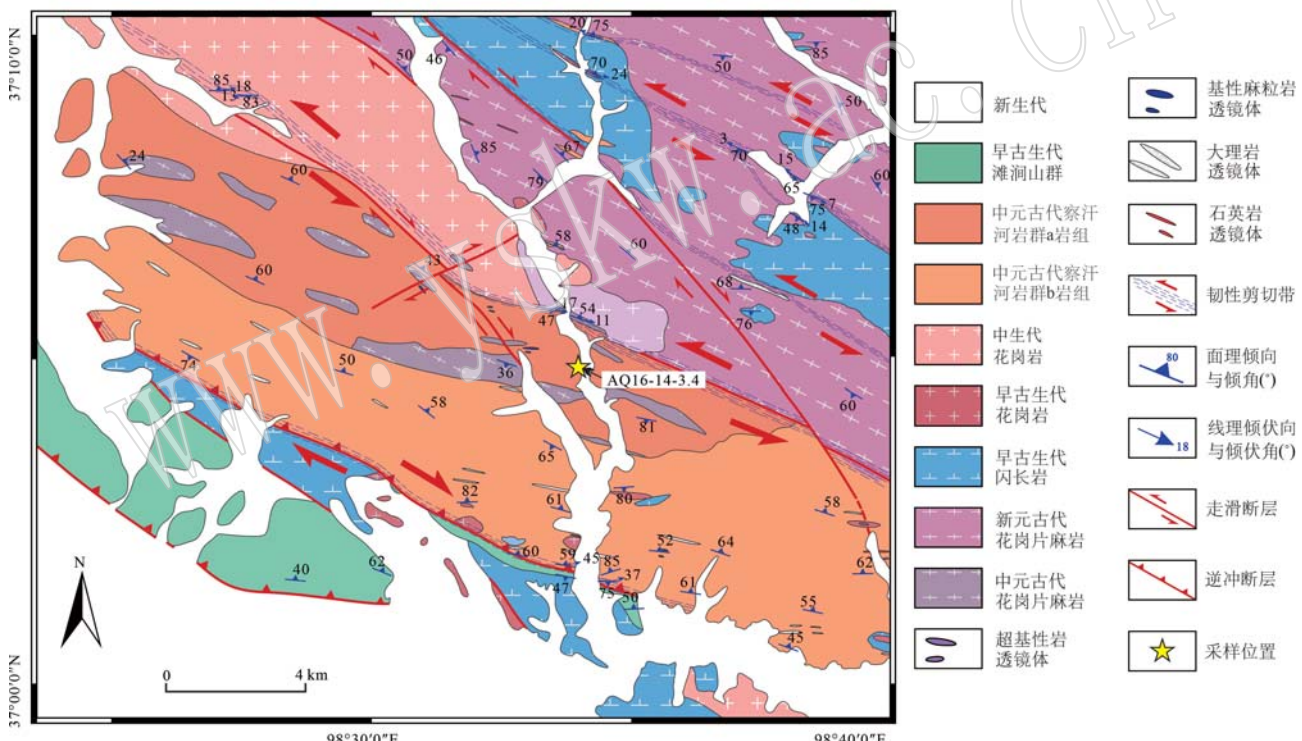


图 2 乌兰地区地质图

Fig. 2 Geological map of Wulan area

中出露的麻粒岩(石榴夕线堇青石片麻岩)为研究对象,开展了详细的岩相学、相平衡模拟和年代学研究,结合已有研究资料,来进一步限定欧龙布鲁克地块的性质和经历的构造热演化历史,为区域构造格局的重建提供依据。

1 区域地质

位于欧龙布鲁克地块北部的南祁连地区,主要由巴龙贡噶尔组和不整合于其上的晚古生代-中生

代沉积岩组成。巴龙贡噶尔组下部为灰色、浅灰紫色千枚岩夹硅质灰岩透镜体,中部为浅灰绿色硬砂岩夹板岩及凝灰岩,上部为紫色、灰绿色硬砂岩夹板岩、黄绿色硅质岩沉积(牛广智等,2016)。巴龙贡噶尔组原定为下志留统(青海省地质局,1991),后来的研究显示其主体形成时代可能不是志留系(白春东等,2019),碎屑岩中获得的最年轻的碎屑锆石年龄为约550 Ma,因此,巴龙贡噶尔组的形成时代还需再确定或解体。该单元北部木里地区,出露蛇纹石化橄榄岩、辉石岩、辉长岩和枕状熔岩等组成的蛇绿混杂岩,辉长岩的锆石年龄为520~470 Ma(Yan et al.,2019;张帅等,2022),玄武岩具有N-MORB的地球化学特征,其向东可与拉脊山蛇绿混杂岩相连,向西延至党河南山一带(Song et al.,2017)。拉脊山-木里-党河南山蛇绿混杂岩带被认为是南祁连俯冲增生杂岩带与(中)祁连地块的分界。

欧龙布鲁克地块呈狭长的条带状分布于全吉山-德令哈-乌兰一带,其基底岩系主要由古元古代德令哈杂岩、达肯大坂岩群及中元古代万洞沟群组成(陆松年,2002;陆松年等,2002;Lu et al.,2008)。德令哈杂岩形成时代为2.4~2.3 Ga,达肯大坂岩群形成时代可能略晚于德令哈杂岩,但二者共同经历了1.96~1.8 Ga的区域变质事件(王勤燕等,2008;Chen et al.,2009,2012,2013;Gong et al.,2012;Liao et al.,2014)。欧龙布鲁克地块西段和德令哈地区分别出露 $1\ 776\pm33$ Ma的环斑花岗岩和 $1\ 712\pm47$ Ma的基性岩侵入体(肖庆辉等,2003;廖梵汐等,2012;Liao et al.,2018)。未变质的全吉群及早古生代以来的沉积岩系呈角度不整合覆盖于古元古代变质基底之上。近年来在乌兰地区识别出一些中新元古代正片麻岩(Wang et al.,2016,2021a,2021b;Xiao et al.,2020)和中元古代副变质岩(Yu et al.,2019;Wang et al.,2019,2021b),特别是普遍发育有早古生代岩浆和变质事件的记录(李秀财等,2015a,2015b;孙娇鹏等,2015;Wang et al.,2018),与欧龙布鲁克地块主要岩石组成及变质演化历史等均有较大差异。综合前人的研究及区域地质资料,我们认为该地区是一套叠加在中新元古代岩石之上的早古生代岩浆-变质岩组合,因此,本文将这一地区的岩石从原欧龙布鲁克地块分离出来,划分为一个独立的岩石构造单元,称为“乌兰北变质-岩浆杂岩带”。

位于欧龙布鲁克地块南部的柴北缘HP-UHP变

质带西起鱼卡地区,东至都兰沙柳河地区(图1),以含榴辉岩、石榴橄榄岩及相关片麻岩为特征,其主体被认为是大陆深俯冲的产物(杨经绥等,1998;Song et al.,2003,2005,2006;张建新等,2004,2007,2009a,2009b;Mattinson et al.,2007;Zhang et al.,2008,2009;Zhang et al.,2010;Yu et al.,2013b;于胜尧等,2014)。该变质带不同地区的榴辉岩、副片麻岩及石榴橄榄岩中相继发现柯石英包、柯石英假像、金刚石等确凿的超高压变质作用证据(Song et al.,2003,2005;Zhang et al.,2009;张建新等,2009a;Zhang et al.,2010),表明柴北缘作为整体曾经被俯冲到80~150 km的地幔深度。带内榴辉岩相变质年龄介于460~420 Ma之间(Mattinson et al.,2006;Zhang et al.,2010,2017;Song et al.,2010,2012,2014;Yu et al.,2013b)。

2 野外关系及岩相学特征

在乌兰北部的察汗河村-哈里哈图地区,岩石单元主体呈北西西向展布,主要由中新元古代的副变质岩系(察汗河岩群)、中新元古代多期次的变质长英质侵入岩、古生代和早中生代岩浆岩及少量滩间山群浅变质火山-沉积岩组成(图2)。其中察汗河岩群b岩组和中-新元古代正片麻岩普遍遭受了早古生代变质作用的叠加,本文研究的石榴夕线堇青石片麻岩(AQ16-14-3.4)采自乌兰北变质-岩浆杂岩带中的察汗河岩群a岩组,采样位置详见图2。

样品石榴夕线堇青石片麻岩主要由石榴子石、夕线石、堇青石、斜长石、黑云母、钛铁矿、石英及少量钾长石组成,副矿物有独居石和锆石。石榴子石中发育石英包裹体,石榴子石较为破碎,且以裂隙中发育晚期矿物堇青石为特征(图3a~3c)。岩相学观察显示,石榴子石已被部分分解,被分解的石榴子石边部被夕线石和黑云母环绕,也有石榴子石边部被斜长石和夕线石环绕(图3a)。夕线石有两种产出状态,或呈较大的板柱状分布在基质中,或呈细小粒状与细小片状黑云母环绕石榴子石的边部生长(图3b)。堇青石主要沿石榴子石的裂隙发育,堇青石内部可见黑云母、夕线石、石英和石榴子石包裹体发育(图3a~3d)。斜长石主要呈两种产出状态,环绕石榴子石边部,且包裹早期夕线石生长,或呈细小粒状与石英和夕线石分布在石榴子石的边部(图3c、3d)。

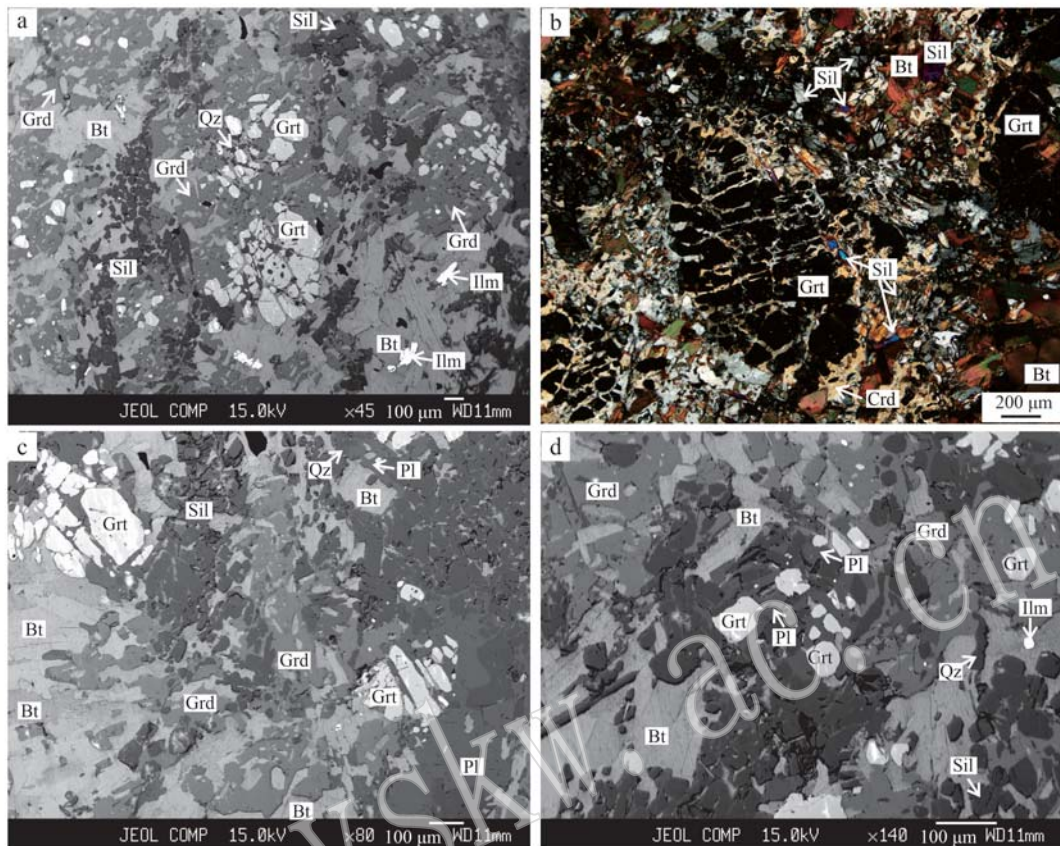


图3 石榴夕线堇青石片麻岩(AQ16-14-3.4)的显微照片及背散射图像

Fig. 3 Photomicrographs and back-scattered electron (BSE) images of garnet-sillimanite-cordierite gneiss from Wulan area (AQ16-14-3.4)

a—石榴子石较为破碎,一些石榴子石已被部分或完全分解,石榴子石边部被细小粒状夕线石环绕(BSE); b—基质中可见粗粒板状夕线石发育,晚期堇青石沿石榴子石裂隙发育,黑云母正交偏光下呈深褐色或黄绿色(CPL); c—斜长石环绕石榴子石发育,且包裹夕线石,大小不同的黑云母呈片状与堇青石共生(BSE); d—破碎的石榴子石边部可见细小的斜长石和夕线石环绕(BSE)

a—the broken garnet is partially or completely decomposed, and the garnet is surrounded by fine sillimanite(BSE); b—coarse plate-like sillimanite in the matrix, and cordierite occurs along cracks of garnet(CPL); c—plagioclase with sillimanite inclusion occurs around garnet, and different biotite with different size occur with cordierite(BSE); d—garnet is surrounded by Pl+Sil+Bt(BSE)

黑云母在正交偏光下呈深褐色或绿色,背散射图像显示大小不同的片状黑云母常与夕线石、堇青石等矿物产出(图3b)。钛铁矿主要呈不规则状或粒状被黑云母包裹,或分布于片状黑云母粒间,或与夕线石等环绕石榴子石的边部生长(图3a、3d)。石英作为包裹体产出于石榴子石中,或呈细小颗粒与夕线石、斜长石和堇青石等共生。根据岩相学观察,石榴夕线堇青石片麻岩的矿物组合可分为3期(M1、M2、M3),M1阶段矿物组合有斜长石±钾长石+石榴子石+夕线石+石英,M2阶段矿物组合有斜长石±钾长石+石榴子石+夕线石+石英+钛铁矿+黑云母,M3阶段矿物组合有堇青石+黑云母+钛铁矿+石英+石榴子石+斜长石±钾长石。文中的主要矿物简写为:Grt(石榴子石), Sil(夕线石), Pl(斜长石),

Qz(石英), Rt(金红石), Ilm(钛铁矿), Crd(堇青石), Kfs(钾长石), Bt(黑云母), 详见 Whitney 和 Evans (2010)。

3 矿物化学

该样品的矿物化学成分测试在中国地质科学院地质研究所完成,分析使用的仪器为日本电子(JEOL) JXA-8100型电子探针,测试电压为15 kV,束流20 nA,束斑5 μm,对于较小的矿物使用的束斑1~5 μm不等,摄谱时间10 s,背景分析时间5 s。使用ZAF程序校正,标样使用SPI公司的组合标样。石榴夕线堇青石片麻岩(样品AQ16-14-3.4)的代表性矿物化学成分见表1。

表1 石榴夕线堇青石片麻岩的矿物化学成分
Table 1 Representative mineral compositions of grt-sill-crd gneiss

 $w_B/\%$

矿物	grt	grt	crd	crd	bt	bt	bt	bt	pl	pl
产状	grt-c	grt-r	crd-in-crack	crd-in-crack	bt-near-grt	bt-near-grt	bt-in-crd	bt-in-crack	pl-around-grt	pl-near-sil
SiO ₂	37.57	37.43	48.44	48.46	34.48	34.55	34.67	35.02	60.22	61.14
TiO ₂	0.00	0.00	0.00	0.00	3.39	3.40	3.05	1.27	0.02	0.00
Al ₂ O ₃	20.48	20.29	32.54	32.79	20.08	19.85	20.09	21.52	24.39	24.10
Cr ₂ O ₃	0.02	0.03	0.05	0.04	0.06	0.00	0.10	0.16	0.00	0.00
Fe ₂ O ₃	0.00	0.00	0.30	0.06	0.00	0.00	0.00	0.00	0.07	0.10
FeO	34.54	32.49	12.01	11.93	23.02	23.72	22.64	22.12	0.00	0.00
MnO	2.98	6.61	0.69	0.66	0.13	0.17	0.12	0.20	0.00	0.04
MgO	2.91	1.50	5.38	5.48	4.78	4.95	5.11	6.34	0.00	0.00
CaO	1.19	1.16	0.01	0.01	0.04	0.01	0.05	0.10	7.14	6.19
Na ₂ O	0.02	0.03	0.22	0.19	0.32	0.33	0.35	0.32	7.41	7.64
K ₂ O	0.00	0.00	0.00	0.01	8.89	9.08	9.01	8.86	0.05	0.14
O	12	12	18	18	11	11	11	11	8	8
Si	3.04	3.05	5.02	5.02	2.67	2.66	2.68	2.67	2.70	2.73
Ti	0.00	0.00	0.00	0.00	0.20	0.20	0.18	0.07	0.00	0.00
Al	1.95	1.95	3.98	4.00	1.83	1.80	1.83	1.93	1.29	1.27
Cr	0.00	0.00	0.00	0.00	0.00	0.00	0.01	0.01	0.00	0.00
Fe ³⁺	0.00	0.00	0.02	0.01	0.00	0.00	0.00	0.00	0.00	0.00
Fe ²⁺	2.34	2.22	1.04	1.03	1.49	1.53	1.46	1.41	0.00	0.00
Mn	0.20	0.46	0.06	0.06	0.01	0.01	0.01	0.01	0.00	0.00
Mg	0.35	0.18	0.83	0.85	0.55	0.57	0.59	0.72	0.00	0.00
Ca	0.10	0.10	0.00	0.00	0.00	0.00	0.00	0.01	0.34	0.30
Na	0.00	0.01	0.04	0.04	0.05	0.05	0.05	0.05	0.64	0.66
K	0.00	0.00	0.00	0.00	0.88	0.89	0.89	0.86	0.00	0.01
Sum	7.99	7.97	11.00	11.00	7.68	7.71	7.70	7.74	4.98	4.97
X_{Alm}	0.78	0.75								
X_{Prp}	0.12	0.06								
X_{Grs}	0.03	0.03								
X_{Spes}	0.07	0.15								
X_{Mg}	0.13	0.08	0.44	0.45	0.27	0.27	0.29	0.34		
An									0.35	0.31

$X_{\text{Alm}} = \text{Fe}^{2+}/(\text{Fe}^{2+} + \text{Mn} + \text{Mg} + \text{Ca})$; $X_{\text{Prp}} = \text{Mg}/(\text{Fe}^{2+} + \text{Mn} + \text{Mg} + \text{Ca})$; $X_{\text{Grs}} = \text{Ca}/(\text{Fe}^{2+} + \text{Mn} + \text{Mg} + \text{Ca})$; $X_{\text{Spes}} = \text{Mn}/(\text{Fe}^{2+} + \text{Mn} + \text{Mg} + \text{Ca})$; $X_{\text{Mg}} = \text{Mg}/(\text{Mg} + \text{Fe}^{2+})$; An = Ca/(Ca + Na + K); A-c: 矿物 A 的核部; A-r: 矿物 A 的边部; A-in-crack: 石榴子石裂隙中发育的矿物 A; A-near-grt: 环绕石榴子石边部生长的矿物 A; A-in-crd: 堇青石中的矿物包体 A; A-around-grt: 环绕石榴子石生长的矿物 A; A-near-sil: 矿物 A 与环绕石榴子石边部生长的 sil 共生。

3.1 石榴子石

石榴子石变斑晶的代表性化学成分测试结果详见表1, 石榴子石铁铝榴石端员组分为0.75~0.79, 镁铝榴石端员组分为0.06~0.12, 钙铝榴石端员组分为0.03, 锰铝榴石端员组分为0.07~0.16。石榴子石的 X_{Mg} 值[$\text{Mg}/(\text{Mg} + \text{Fe}^{2+})$]为0.08~0.13。石榴子石核部镁铝榴石端员组分为0.11~0.12, 而边部镁铝榴石端员组分在0.06~0.07之间变化。

3.2 黑云母

黑云母的 X_{Mg} 值[$\text{Mg}/(\text{Mg} + \text{Fe}^{2+})$]在0.26~0.27之间变化, TiO_2 含量在3.38%~3.42%之间变

化。岩石中黑云母有3种产出状态:环绕石榴子石边部生长的黑云母具有高的 TiO_2 含量和低的 X_{Mg} 值;堇青石中的包裹体黑云母相对于石榴子石边部的黑云母具有较低的 TiO_2 含量和较高的 X_{Mg} 值;与堇青石共生的黑云母具有最低的 TiO_2 含量和最高的 X_{Mg} 值(图4a)。

3.3 长石和堇青石

斜长石主要有两类,环绕石榴子石边部,且包裹早期夕线石的斜长石An值[$\text{Ca}/(\text{Ca} + \text{Na} + \text{K})$]在0.33~0.35之间变化,环绕在石榴子石边部且与夕线石平衡共生的斜长石An值为0.31(图4b)。堇青

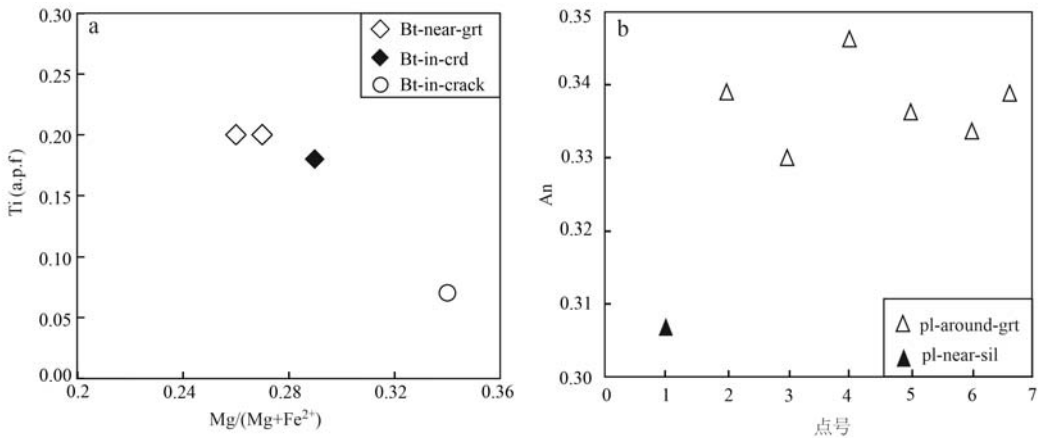


图4 石榴夕线堇青石片麻岩(AQ16-14-3.4)中的黑云母 $Ti/(Mg+Fe^{2+})$ 图解(a)和斜长石不同部位的 An 值(b)

Fig. 4 $Ti/(Mg+Fe^{2+})$ diagram of biotite (a) and An value diagram of different plagioclase in garnet-sillimanite-cordierite gneiss (b) from Wulan area (AQ16-14-3.4)

石沿石榴子石裂隙生长, 堇青石的 X_{Mg} 值在 0.43~0.46 之间变化。斜长石和堇青石的代表性化学成分测试结果详见表 1。

4 变质作用温压条件

本文在获取实测全岩成分基础上, 利用 GeoPS v3.4 程序 (Xiang and Connolly, 2022), 选择 NCKF-MASHTO [$Na_2O-CaO-K_2O-FeO-MgO-Al_2O_3-SiO_2-H_2O-TiO_2-O(Fe_2O_3)$] 体系对乌兰北部石榴夕线堇青石片麻岩(样品 AQ16-14-3.4)开展了相平衡模拟计算, 以确定该岩石的变质条件及 $p-T$ 演化轨迹。

本文通过 $T-M_{H_2O}$ 和 $T-M_0$ 图及实测矿物成分等值线图共同确定模拟所需的 O 和 H_2O 的摩尔分数, 所确定的 O 和 H_2O 的摩尔分数需保证所观察到的最终矿物组合恰好在固相线之上可以稳定存在 (Korhonen et al., 2012; Li and Wei, 2016)。假设 P_2O_5 主要形成磷灰石, 并对 CaO 含量做出相应调整, 归一后的全岩成分为: SiO_2 58.51%, Al_2O_3 15.55%, CaO 2.23%, MgO 4.8%, FeO 12.26%, K_2O 1.47%, Na_2O 1.51%, TiO_2 0.96%, O 0.01%, H_2O 2.7% (摩尔分数), 利用该全岩成分模拟峰期 $p-T$ 条件及退变质阶段的 $p-T$ 演化轨迹。

模拟采用的内部一致性热力学数据库为 Holland 和 Powell (2011) 发表的版本 ds62, 矿物活度模型为: 黑云母 (Bt; White et al., 2014), 石榴子石 (Grt; White et al., 2014), 绿泥石 (Chl; White et al., 2014), 堇青石 (Crd; White et al., 2014), 绿帘

石 (Ep; Holland and Powell, 2011), 斜长石 (Pl; Holland and Powell, 2003), 钾长石 (Kfs; Holland and Powell, 2003), 钛铁矿 (Ilm; White et al., 2014), 熔体 (Liq; White et al., 2014), 白云母 (Ms; White et al., 2014), 斜方辉石 (Opx; White et al., 2014), 尖晶石 (Spl; White et al., 2002), 十字石 (St; White et al., 2014), 夕线石 (Sil), 石英 (Qz), 金红石 (Rt), 蓝晶石 (Ky) 为纯端员组分。

图 5 为石榴夕线堇青石片麻岩(样品 AQ16-14-3.4)在 $p=0.2\sim1.2$ GPa, $t=600\sim1000^\circ C$ 范围内的 $p-T$ 视剖面图。视剖面图显示, 金红石在 $p>0.7$ GPa 的条件下稳定存在; 黑云母大致稳定在 $t<800^\circ C$ 的范围内; 堇青石在 $p<0.55$ GPa 的条件下稳定存在; 钛铁矿大致稳定存在于 $p<0.9$ GPa 的区域内; 固相线出现在温度范围 $680\sim790^\circ C$ 之间; 石英和斜长石稳定存在于视剖面图中大部分区域; 尖晶石大致存在于 $p<0.7$ GPa, $t>840^\circ C$ 范围内。实测斜长石 An 值 ($An=0.31\sim0.35$) 等值线投入 Grt+Kfs+Ky+Rt+Pl+Qz+Liq 和 Grt+Kfs+Sil+Rt+Pl+Qz+Liq 矿物组合稳定区域内, 随着温度的升高 An 值逐渐变大, 随着压力的升高 An 值逐渐变小; 石榴子石的钙铝榴石端员成分等值线 ($Gr=0.03\sim0.04$) 位于 $p<0.9$ GPa 的区域内, 而石榴子石的镁铝榴石端员成分等值线 ($Py=0.08\sim0.12$) 位于 $p<0.4$ GPa, $t<850^\circ C$ 的区域内。

岩相学观察显示, 该岩石的矿物组合分为 3 期 (M1、M2、M3), M1 阶段矿物组合有 $Pl\pm Kfs+Grt+Sill+Qz$, M2 阶段矿物组合有 $Pl\pm Kfs+Grt+Sill+Qz+Ilm+$

Bt, M3 阶段矿物组合有 Crd + Bt + IIm + Qz + Grt + Pl ± Kfs。斜长石 An 值投在了 Grt+Kfs+Ky+Rt+Pl+Qz+Liq 和 Grt+Kfs+Sil+Rt+Pl+Qz+Liq 矿物组合稳定区域内, 推测该岩石的峰期温压条件为 $p>0.92$ GPa, $t>790^{\circ}\text{C}$, 石榴子石的镁铝榴石等值线投在了 M3 阶段矿物组合 Bt+Crd+Grt+IIm+Kfs+Pl+Qz 稳定存在的区域, 这可能

因为石榴子石比较破碎, 受晚期退变质作用的改造显著, 使得石榴子石成分发生了重置, 镁铝榴石的成分仅是对退变质阶段的温度条件的反映。根据岩相学观察的 3 期矿物组合和矿物成分等值线, 推测该岩石峰期之后经历了略增温降压的顺时针 p - T 演化轨迹(图 5 粉色粗箭头)。

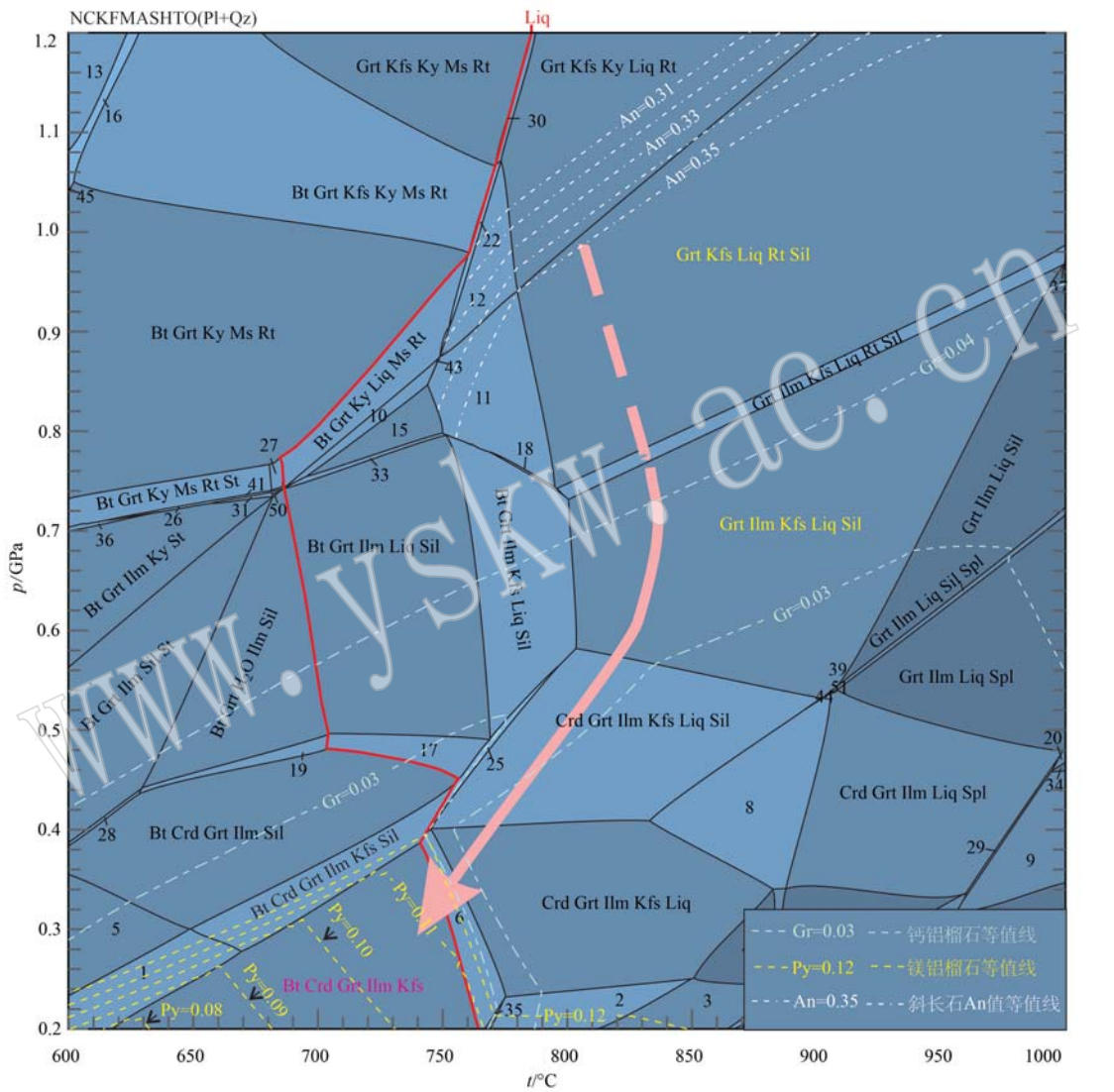


图 5 石榴夕线堇青石片麻岩(AQ16-14-3.4) p - T 视剖面图及 p - T 演化轨迹

Fig. 5 p - T pseudosection and p - T path for garnet-sillimanite-cordierite gneiss (AQ16-14-3.4)

粉色粗箭头代表峰期及退变质 p - T 演化轨迹; 虚线代表推测的 p - T 轨迹; $\text{Gr}=\text{Ca}/(\text{Mg}+\text{Fe}^{2+}+\text{Ca})$; $\text{Py}=\text{Mg}/(\text{Mg}+\text{Fe}^{2+}+\text{Ca})$; $\text{An}=\text{Ca}/(\text{Ca}+\text{Na})$; 红色实线为固相线

light pink arrow is the p - T path after peak of pressure; dotted light pink line is the supposed p - T path; $\text{Gr}=\text{Ca}/(\text{Mg}+\text{Fe}^{2+}+\text{Ca})$; $\text{Py}=\text{Mg}/(\text{Mg}+\text{Fe}^{2+}+\text{Ca})$; $\text{An}=\text{Ca}/(\text{Ca}+\text{K}+\text{Na})$; red line is the solidus line

5 年代学研究

5.1 测试方法

对石榴夕线堇青石片麻岩(AQ16-14-3.4)分别开展了锆石和独居石U-Pb同位素定年工作。锆石U-Pb同位素定年在北京燕都中实测试技术有限公司利用LA-ICP-MS完成,采用New Ware UP213激光剥蚀系统和德国耶拿M90的ICP-MS。采用氦气作为载气、氩气为补偿气,通过一个Y型接头将两者混合然后进入ICP。每个数据包括大约20~30 s的空信号和50 s的样品信号。采用软件ICPMSCal(Liu et al., 2008, 2010)对分析数据进行离线处理。详细的仪器操作条件和数据处理方法同Liu等(2008, 2010)。本次分析使用的剥蚀直径为30 μm,采用锆石标准91500作外标,每分析5~10个样品点,分析2次91500,并对Plesovice分析一次。对于U-Th-Pb同位素比值漂移,根据91500的变化采用线性内插的方式进行校正(Liu et al., 2010)。样品的U-Pb年龄谐和图绘制和加权平均年龄计算采用Isoplot/Ex_ver3(Ludwig, 2003)完成,使用Andersen(2002)方法进行普通铅的校正。

独居石LA-ICP-MS U-Pb同位素定年在北京科荟测试技术有限公司完成,分析所用仪器为Analytik Jena PQMS Elite型ICP-MS和配套的RESolution 193 nm准分子激光剥蚀系统。分析过程中,以He为载气,分析时的激光剥蚀束斑为16 μm,频率为6 Hz,能量密度约为8 J/cm²。激光剥蚀采样使用单点剥蚀,测试前使用NIST 610调试仪器状态,标样44 069为外标,每分析10个样品点,分析2次44 069,数据处理采用ICPMSCal程序(Liu et al., 2010),独居石年龄谐和图利用Isoplot/Ex_ver3(Ludwig, 2003)获得。

5.2 锆石和独居石特征

锆石多以浑圆状和椭圆状为主,粒径90~280 μm不等,Th/U值介于0.01~0.53之间。CL图像显示部分锆石具有核-边结构,核部多呈不规则状,具有振荡环带,显示碎屑锆石的特征,边部无明显内部结构或呈补丁状结构,显示变质锆石特征(图6a)。

独居石多呈浑圆状或不规则状,粒径70~300 μm不等,BSE图像显示部分独居石颗粒具有暗色的核和灰色的边,核部多呈不规则,边部无明显内部结构或呈补丁状结构,部分独居石中可见矿物包裹体发育(图6b)。

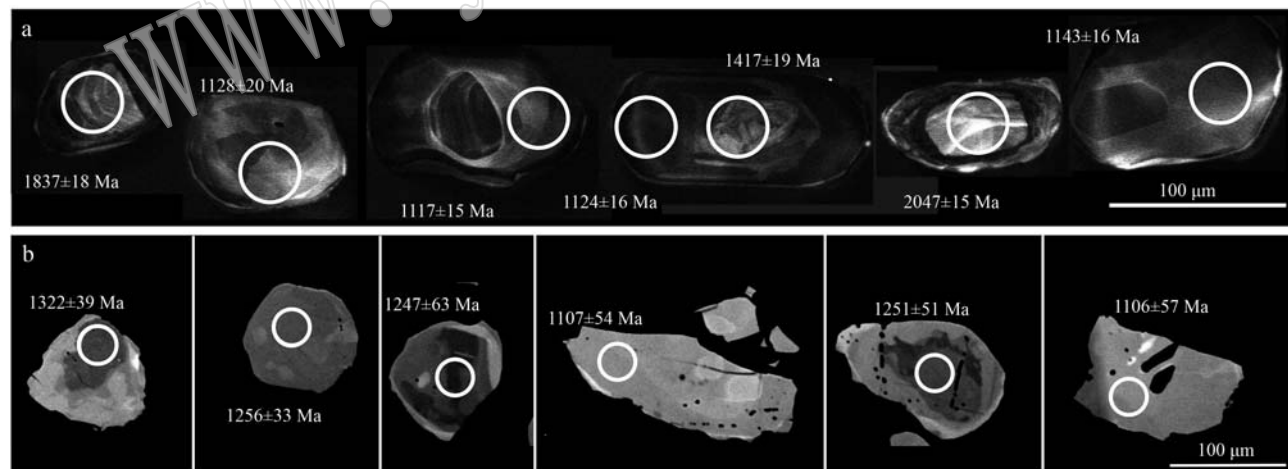


图6 石榴夕线堇青石片麻岩(AQ16-14-3.4)中的锆石CL图像(a)和独居石背散射图像(b)

Fig. 6 CL image of zircons (a) and BSE image of monazites (b) from garnet-sillimanite-cordierite gneiss (AQ16-14-3.4)

5.3 锆石和独居石U-Pb定年结果

对该样品共进行了40个锆石数据点测定,其中碎屑核给出的²⁰⁷Pb/²⁰⁶Pb表面年龄变化在1 417±22 Ma和2 261±26 Ma之间,而锆石边给出的²⁰⁷Pb/²⁰⁶Pb表面年龄变化在1 103±15 Ma和1 183±14 Ma之间(表2),且它们的Th/U值大部分小于0.1,锆石边部

数据点拟合出了一条很好的不一致线,得到的上交点年龄为1 133±14 Ma(MSWD=1.18, 图7a),与1 123±7 Ma(MSWD=0.57)的²⁰⁷Pb/²⁰⁶Pb加权平均年龄在误差范围内一致。我们认为1 133±14 Ma的上交点年龄应代表了其变质时代。

对该样品共进行了40个独居石数据点测定(表3,

表2 样品AQ16-14-3.4中锆石LA-ICP-MS U-Pb定年分析结果
Table 2 Zircon U-Pb isotope data obtained by LA-ICP-MS for sample AQ16-14-3.4

测点号	$w_B/10^{-6}$		Th/U	$^{207}\text{Pb}/^{206}\text{Pb}$		$^{207}\text{Pb}/^{235}\text{U}$	1σ	$^{206}\text{Pb}/^{238}\text{U}$		1σ	$^{207}\text{Pb}/^{206}\text{Pb}$		1σ	$^{207}\text{Pb}/^{235}\text{U}$		1σ	$^{206}\text{Pb}/^{238}\text{U}$		1σ	
	Th	U																		
1	36	712	0.05	0.076 426	0.000 669	1.819 761	0.021 782	0.172 089	0.001 612	1.106	18	1.053	8	1.024	9					
2	90	787	0.11	0.088 722	0.000 862	2.505 899	0.028 350	0.203 995	0.001 397	1.398	14	1.274	8	1.197	7					
3	30	964	0.03	0.077 254	0.000 600	1.918 610	0.018 056	0.179 555	0.001 229	1.128	10	1.088	6	1.065	7					
4	57	412	0.14	0.092 067	0.000 846	2.440 979	0.025 557	0.191 576	0.001 130	1.469	18	1.255	8	1.130	6					
5	54	469	0.11	0.077 843	0.000 642	2.058 955	0.021 057	0.191 284	0.001 387	1.143	16	1.135	7	1.128	8					
6	110	318	0.35	0.126 329	0.001 032	6.029 256	0.059 995	0.345 209	0.002 407	2.047	15	1.980	9	1.912	12					
7	120	1400	0.09	0.078 254	0.000 575	1.995 114	0.020 157	0.184 487	0.001 511	1.154	15	1.114	7	1.091	8					
8	125	967	0.13	0.077 155	0.000 621	1.990 035	0.019 014	0.186 551	0.001 195	1.125	17	1.112	6	1.103	6					
9	18	727	0.03	0.080 209	0.000 708	2.134 405	0.026 680	0.192 200	0.001 683	1.267	18	1.160	9	1.133	9					
10	39	693	0.06	0.089 525	0.000 885	2.560 802	0.048 083	0.205 490	0.002 865	1.417	19	1.290	14	1.205	15					
11	21	946	0.02	0.077 064	0.000 628	1.892 339	0.017 547	0.177 734	0.001 130	1.124	16	1.078	6	1.055	6					
12	162	304	0.53	0.096 025	0.000 889	3.400 125	0.045 304	0.255 567	0.002 262	1.550	17	1.504	10	1.467	12					
13	48	753	0.06	0.086 334	0.000 645	2.387 729	0.026 456	0.199 958	0.001 738	1.346	15	1.239	8	1.175	9					
14	100	574	0.17	0.076 835	0.000 608	2.008 470	0.019 033	0.189 175	0.001 324	1.117	15	1.118	6	1.117	7					
15	52	610	0.09	0.076 551	0.000 607	1.839 743	0.020 818	0.173 825	0.001 563	1.109	15	1.060	7	1.033	9					
16	172	415	0.41	0.091 237	0.001 067	2.507 676	0.030 818	0.198 999	0.001 334	1.452	22	1.274	9	1.169	7					
17	165	866	0.19	0.091 440	0.000 748	2.500 519	0.025 353	0.197 602	0.001 333	1.457	16	1.272	7	1.162	7					
18	197	460	0.43	0.142 703	0.002 151	6.873 342	0.179 138	0.338 055	0.005 774	2.261	26	2.095	23	1.877	28					
19	141	800	0.18	0.095 183	0.000 809	3.263 318	0.033 353	0.247 596	0.001 606	1.532	16	1.472	8	1.426	8					
20	159	357	0.45	0.077 199	0.000 752	2.040 888	0.022 752	0.191 279	0.001 520	1.128	20	1.129	8	1.128	8					
21	3	368	0.01	0.069 149	0.000 695	1.277 388	0.013 808	0.133 711	0.000 935	903	20	836	6	809	5					
22	143	495	0.29	0.112 278	0.001 127	4.237 166	0.075 149	0.270 182	0.003 255	1.837	18	1.681	15	1.542	17					
23	38	710	0.08	0.076 945	0.000 572	2.028 768	0.018 567	0.190 756	0.001 326	1.120	19	1.125	6	1.125	7					
24	17	2704	0.01	0.076 687	0.000 507	1.852 004	0.018 186	0.174 676	0.001 444	1.122	14	1.064	6	1.038	8					
25	24	536	0.04	0.076 680	0.000 592	1.991 777	0.019 857	0.187 981	0.001 449	1.122	15	1.113	7	1.110	8					
26	3	453	0.01	0.073 339	0.000 623	1.651 192	0.016 651	0.163 006	0.001 205	1.033	17	990	6	973	7					
27	128	756	0.17	0.076 310	0.000 579	1.872 475	0.020 042	0.177 525	0.001 497	1.103	15	1.071	7	1.053	8					
28	23	979	0.02	0.074 289	0.000 576	1.662 367	0.016 954	0.161 851	0.001 196	1.050	15	994	6	967	7					
29	80	722	0.11	0.077 063	0.000 665	1.965 170	0.019 395	0.184 609	0.001 226	1.124	17	1.104	7	1.092	7					
30	39	763	0.05	0.077 403	0.000 706	2.017 388	0.023 547	0.188 670	0.001 636	1.131	14	1.121	8	1.114	9					
31	71	691	0.10	0.093 021	0.000 839	2.904 148	0.031 486	0.225 832	0.001 528	1.489	17	1.383	8	1.313	8					
32	122	515	0.24	0.104 975	0.000 853	3.918 557	0.049 061	0.269 543	0.002 409	1.714	15	1.618	10	1.538	12					
33	95	195	0.49	0.124 763	0.000 982	6.343 787	0.063 367	0.368 254	0.002 864	2.026	13	2.025	9	2.021	13					
34	16	1156	0.01	0.076 615	0.000 536	1.895 457	0.022 055	0.178 867	0.001 680	1.122	13	1.079	8	1.061	9					
35	23	1292	0.02	0.076 549	0.000 517	1.922 590	0.018 280	0.181 696	0.001 342	1.109	14	1.089	6	1.076	7					
36	14	1211	0.01	0.079 468	0.000 578	2.107 998	0.020 686	0.191 941	0.001 406	1.183	14	1.151	7	1.132	8					
37	5	489	0.01	0.076 957	0.000 610	1.792 213	0.017 286	0.168 560	0.001 159	1.120	19	1.043	6	1.004	6					
38	16	718	0.02	0.077 177	0.000 636	1.926 864	0.020 433	0.180 796	0.001 493	1.126	17	1.090	7	1.071	8					
39	201	541	0.37	0.076 925	0.000 669	1.986 413	0.021 692	0.187 027	0.001 574	1.120	17	1.111	7	1.105	9					
40	184	438	0.42	0.077 299	0.000 740	1.982 437	0.022 153	0.185 737	0.001 455	1.129	19	1.110	8	1.098	8					

同位素年龄/Ma

表3 样品AQ16-14-3.4独居石LA-ICP-MS U-Pb定年分析结果
Table 3 Monazite U-Pb isotope data obtained by LA-ICP-MS for sample AQ16-14-3.4

测点号	$w_{\text{B}}/10^{-6}$		$^{207}\text{Pb}/^{206}\text{Pb}$			$^{207}\text{Pb}/^{235}\text{U}$			$^{206}\text{Pb}/^{238}\text{U}$			$^{207}\text{Pb}/^{206}\text{Pb}$			$^{207}\text{Pb}/^{235}\text{U}$			$^{206}\text{Pb}/^{238}\text{U}$		
	Th	U	1σ	$207\text{Pb}/^{235}\text{U}$	1σ	$^{206}\text{Pb}/^{238}\text{U}$	1σ	$^{207}\text{Pb}/^{206}\text{Pb}$	1σ	$^{207}\text{Pb}/^{235}\text{U}$	1σ	$^{206}\text{Pb}/^{238}\text{U}$	1σ	$^{207}\text{Pb}/^{235}\text{U}$	1σ	$^{206}\text{Pb}/^{238}\text{U}$	1σ			
1	6.61	0.44	0.077 610	0.002 252	2.006 326	0.062 822	0.187 935	0.002 847	1.137	58	1.118	21	1.110	15	1.110	21	1.110	15		
2	2.05	0.94	0.083 154	0.002 210	2.439 619	0.081 564	0.212 722	0.004 519	1.273	52	1.254	24	1.243	24	1.243	24	1.243	24		
3	5.53	0.46	0.086 178	0.002 169	2.719 996	0.075 035	0.229 619	0.003 540	1.343	48	1.334	21	1.333	19	1.333	21	1.333	19		
4	4.49	0.35	0.075 808	0.002 766	1.905 339	0.074 245	0.182 800	0.004 238	1.100	72	1.083	26	1.082	23	1.082	26	1.082	23		
5	4.30	0.25	0.074 027	0.002 583	1.901 686	0.073 409	0.185 967	0.003 162	1.043	70	1.082	26	1.099	17	1.099	26	1.099	17		
6	4.81	0.34	0.075 342	0.005 142	1.927 928	0.148 113	0.184 872	0.005 332	1.077	105	1.091	51	1.094	29	1.094	51	1.094	29		
7	1.72	0.58	0.085 291	0.001 688	2.663 992	0.056 280	0.226 158	0.002 274	1.322	39	1.319	16	1.314	12	1.314	16	1.314	12		
8	4.27	0.13	0.075 970	0.002 485	1.903 314	0.054 559	0.183 590	0.002 870	1.094	65	1.082	19	1.087	16	1.087	19	1.087	16		
9	4.49	0.13	0.076 471	0.003 375	1.918 741	0.076 413	0.183 323	0.004 198	1.109	89	1.088	27	1.085	23	1.085	27	1.085	23		
10	6.29	0.48	0.076 385	0.001 823	1.952 581	0.047 447	0.184 987	0.002 326	1.106	48	1.099	16	1.094	13	1.094	16	1.094	13		
11	4.64	0.29	0.076 759	0.002 216	2.000 622	0.059 912	0.188 872	0.003 143	1.117	57	1.116	20	1.115	17	1.115	20	1.115	17		
12	4.52	0.39	0.078 625	0.001 830	1.918 826	0.049 876	0.176 519	0.002 844	1.163	46	1.088	17	1.048	16	1.048	17	1.048	16		
13	4.16	0.27	0.077 241	0.002 839	2.050 646	0.090 571	0.191 332	0.003 162	1.128	73	1.133	30	1.129	17	1.129	30	1.129	17		
14	4.14	0.78	0.082 045	0.001 403	2.416 541	0.048 207	0.212 803	0.002 533	1.256	33	1.248	14	1.244	13	1.244	14	1.244	13		
15	1.51	0.73	0.077 953	0.003 106	2.057 412	0.088 592	0.191 531	0.004 581	1.146	84	1.135	29	1.130	25	1.130	29	1.130	25		
16	4.01	0.23	0.077 240	0.001 836	2.031 694	0.054 260	0.189 967	0.002 415	1.128	47	1.126	18	1.121	13	1.121	18	1.121	13		
17	4.21	0.24	0.078 338	0.002 305	2.063 186	0.058 999	0.191 221	0.002 455	1.155	58	1.137	20	1.128	13	1.128	20	1.128	13		
18	3.82	0.32	0.081 983	0.001 857	2.397 446	0.056 525	0.212 151	0.003 041	1.256	11	1.242	17	1.240	16	1.240	17	1.240	16		
19	3.06	0.10	0.075 931	0.002 343	1.929 029	0.064 262	0.184 830	0.003 111	1.094	61	1.091	22	1.093	17	1.093	22	1.093	17		
20	0.49	0.44	0.082 073	0.002 660	2.417 146	0.096 070	0.213 404	0.005 885	1.247	63	1.248	29	1.247	31	1.247	29	1.247	31		
21	4.03	0.15	0.078 221	0.005 103	2.137 075	0.176 130	0.198 133	0.016 211	1.154	130	1.161	57	1.165	87	1.165	57	1.165	87		
22	4.08	0.46	0.076 460	0.002 075	2.015 031	0.055 545	0.191 084	0.002 846	1.107	54	1.121	19	1.127	15	1.127	19	1.127	15		
23	2.99	0.84	0.082 234	0.002 135	2.414 298	0.058 293	0.213 338	0.004 072	1.251	51	1.247	17	1.247	22	1.247	17	1.247	22		
24	3.63	0.08	0.078 753	0.004 073	1.997 520	0.106 620	0.183 456	0.003 211	1.166	102	1.115	36	1.086	17	1.086	36	1.086	17		
25	3.68	0.36	0.080 661	0.001 951	2.369 464	0.072 555	0.212 270	0.003 893	1.213	48	1.233	22	1.241	21	1.241	22	1.241	21		
26	2.69	0.13	0.077 685	0.006 214	2.006 211	0.146 503	0.189 930	0.006 794	1.139	164	1.118	49	1.121	37	1.121	49	1.121	37		
27	3.56	0.79	0.077 439	0.001 719	2.042 613	0.048 840	0.191 427	0.004 948	1.132	44	1.130	16	1.129	27	1.129	16	1.129	27		
28	0.05	0.05	0.081 389	0.004 049	2.389 396	0.142 716	0.210 292	0.005 915	1.231	97	1.239	43	1.230	32	1.230	43	1.230	32		
29	2.99	0.13	0.075 548	0.003 523	1.928 042	0.097 592	0.184 672	0.003 544	1.083	93	1.091	34	1.092	19	1.092	34	1.092	19		
30	3.57	0.20	0.076 421	0.001 945	1.924 193	0.050 244	0.183 006	0.002 387	1.106	56	1.090	17	1.083	13	1.083	17	1.083	13		
31	3.94	0.75	0.083 564	0.002 433	2.443 806	0.060 886	0.212 399	0.004 488	1.283	53	1.256	18	1.242	24	1.242	18	1.242	24		
32	3.61	0.26	0.072 339	0.002 670	1.383 643	0.053 073	0.138 618	0.002 440	995	106	882	23	837	14	837	23	837	14		
33	2.70	0.07	0.076 848	0.005 416	2.014 588	0.135 499	0.190 676	0.004 239	1.117	141	1.120	46	1.125	23	1.125	46	1.125	23		
34	3.86	0.20	0.077 131	0.002 403	2.031 655	0.057 791	0.192 005	0.002 402	1.124	63	1.126	19	1.132	13	1.132	19	1.132	13		
35	0.30	0.28	0.087 359	0.002 264	2.776 506	0.068 780	0.230 896	0.004 230	1.369	50	1.349	19	1.339	22	1.339	22	1.339	22		
36	1.78	0.15	0.076 987	0.004 993	2.015 383	0.110 267	0.190 967	0.006 875	1.120	134	1.121	37	1.127	37	1.127	37	1.127	37		
37	2.88	0.50	0.084 786	0.002 245	0.929 344	0.029 309	0.079 189	0.001 284	1.311	51	667	15	491	8	491	15	491	8		
38	4.20	0.17	0.078 905	0.007 057	2.064 814	0.169 719	0.189 983	0.002 819	1.169	178	1.137	56	1.121	15	1.121	56	1.121	15		
39	2.87	0.14	0.076 215	0.002 396	1.993 668	0.056 580	0.191 193	0.003 839	1.102	63	1.113	19	1.128	21	1.128	19	1.128	21		
40	3.22	0.45	0.076 238	0.002 282	2.015 872	0.062 857	0.191 554	0.003 538	1.102	60	1.121	21	1.130	19	1.130	21	1.130	19		

图7b),其中暗色的核给出的 $^{207}\text{Pb}/^{206}\text{Pb}$ 表面年龄变化在 $1\ 169\pm178\text{ Ma}$ 和 $1\ 369\pm50\text{ Ma}$ 之间,除去误差较大的数据点,8个数据点给出的 $^{207}\text{Pb}/^{206}\text{Pb}$ 加权平均年龄为 $1\ 255\pm19\text{ Ma}$ (图7c)。灰色的边给出

的 $^{207}\text{Pb}/^{206}\text{Pb}$ 表面年龄变化在 $1\ 043\pm70\text{ Ma}$ 和 $1\ 166\pm102\text{ Ma}$ 之间,除去误差较大数据点,13个数据点给出的 $^{207}\text{Pb}/^{206}\text{Pb}$ 加权平均年龄为 $1\ 125\pm37\text{ Ma}$ (图7d)。

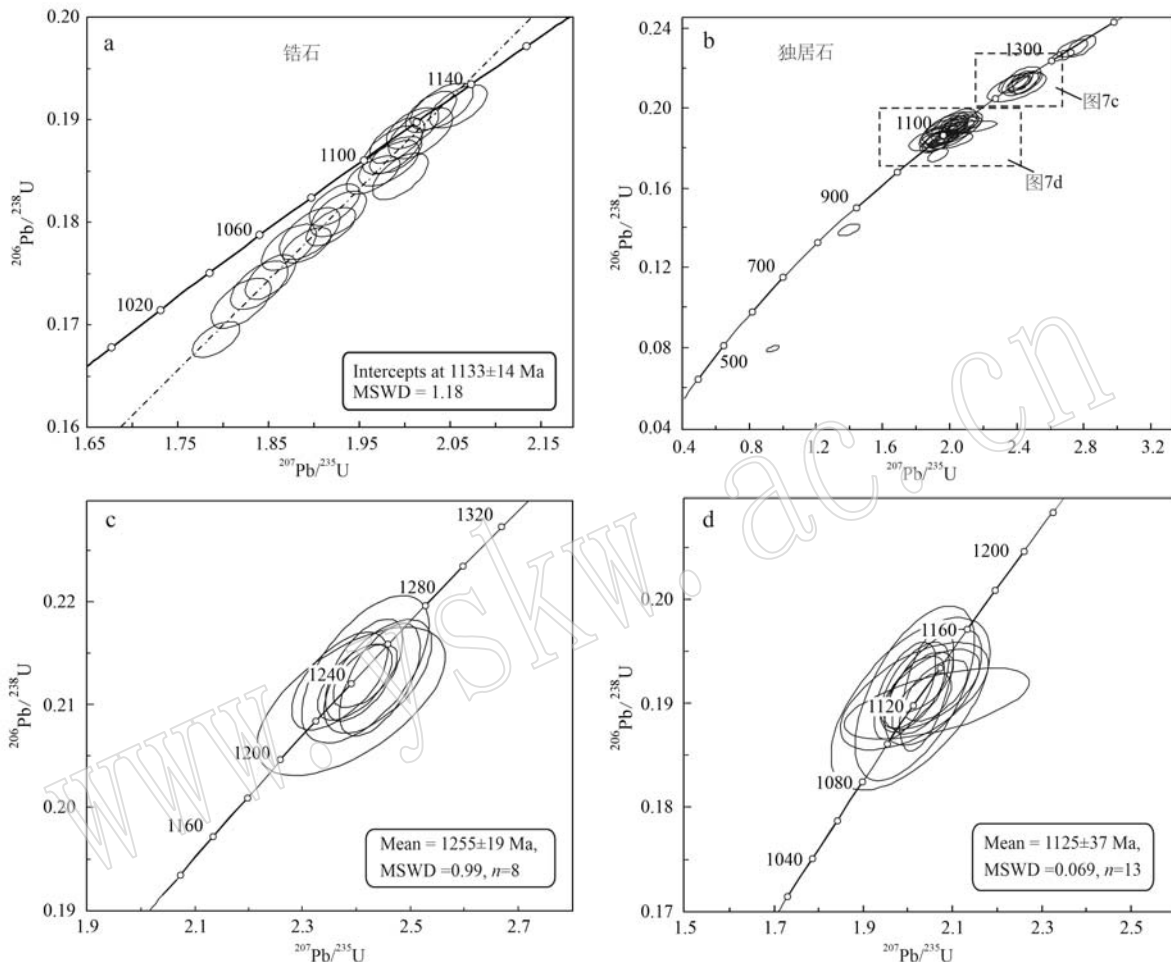


图7 石榴夕线堇青石片麻岩(AQ16-14-3.4)的锆石(a)和独居石(b~d)U-Pb谐和图

Fig. 7 Zircon (a) and monazite (b~d) U-Pb concordia diagrams for garnet-sillimanite-cordierite gneiss (AQ16-14-3.4)

6 讨论

6.1 石榴夕线堇青石片麻岩的变质作用

通常,麻粒岩峰期矿物成分在退变质作用过程中极易被改造(Powell and Holland, 2008; Kelsey and Hand, 2015),本文中石榴夕线堇青石片麻岩中石榴子石的镁铝榴石和钙铝榴石等值线均投在了M3阶段的矿物组合稳定域内,这可能是石榴子石较为破碎,受到了晚期退变质作用的改造,使得石榴子石仅保留了M3阶段的成分信息。因此,本文峰期温压条件主要利用斜长石的An值和峰期的矿物组合共同

确定的。斜长石的An值限制峰期压力最低介于0.92~1.08 GPa之间,温度范围仅由峰期矿物组合限制,推测峰期温度 $t>790^\circ\text{C}$,根据不同阶段的矿物组合和石榴子石镁铝榴石和钙铝榴石等值线,共同限定了该岩石峰期之后略升温降压的顺时针p-T演化轨迹。视剖面图显示,沿着略升温降压的p-T演化轨迹,石榴子石被消耗分解,生成夕线石和斜长石,这与岩相学观察到的石榴子石变斑晶周围被细小的夕线石、斜长石和石英颗粒环绕相一致。随着更晚期的减压降温,石榴子石进一步分解,以黑云母和堇青石的相继出现为特征,与岩相学观察到的石榴子石裂隙中生长堇青石和黑云母相一致。

区域地质资料和近年来的研究表明,乌兰北变质-岩浆杂岩带经历了多期岩浆-变质事件,主要以中元古代末期(约1.2~1.1 Ga)和早古生代(510~410 Ma)的岩浆-变质事件为代表。

中元古代末期的变质作用主要记录在察汗河岩群a岩组中不同类型岩石中,主要以基性、泥质麻粒岩为特征(Yu et al., 2019; Wang et al., 2021b)。Yu等(2019)根据副片麻岩的变质矿物组合(石榴子石+夕线石+黑云母+斜长石±钾长石+石英),计算得到其变质温压条件为0.48~0.58 GPa、652~700°C,认为其代表了中元古代晚期的变质条件。Wang等(2021b)根据泥质片麻岩中石榴子石+堇青石+夕线石+黑云母+斜长石+石英+钛铁矿及富石榴子石岩中尖晶石+石榴子石+黑云母+钛铁矿+夕线石的峰期矿物组合计算得到更高的峰期温度(约840~900°C)和更大范围的压力条件(0.7~1.1 GPa)。

早古生代的变质作用主要记录在察汗河岩群b岩组中不同类型岩石中,以基性、泥质麻粒岩为特征(Wang et al., 2018; Li et al., 2019)。李秀财等(2015a)对区内石榴夕线黑云斜长片麻岩进行温压计算,得到的温压范围为677~696°C、0.32~0.42 GPa; Wang等(2018)运用传统地质温压计对区内的泥质麻粒岩和酸性麻粒岩进行了温压计算,得到了718~729°C、0.46~0.53 GPa的峰期温压条件,并获得了逆时针的p-T轨迹; Li等(2019)通过对泥质麻粒岩及基性麻粒岩的THERMALCALC相平衡模拟,得到了约800~900°C、0.55~0.70 GPa的峰期温压条件和顺时针的p-T演化轨迹。

很显然,本文中相平衡模拟获得的峰期温压条件和p-T演化轨迹与早古生代变质作用特征不同(李秀财等,2015a; Wang et al., 2018; Li et al., 2019),明显高于副片麻岩记录的温压条件(Yu et al., 2019),更接近泥质片麻岩和富石榴子石岩记录的峰期温压条件和p-T演化特征(Wang et al., 2021b),但接近固相线的温压条件有些差异,这可能与麻粒岩相岩石中发生熔体丢失的程度不同有关(White and Powell, 2002)。

6.2 石榴夕线堇青石片麻岩的变质时代

变质锆石可以在麻粒岩相变质作用的进变质阶段生长(Rubatto et al., 2001),也可以在峰期及峰期之后的降温过程中生长(Hoskin and Black, 2000; Kelsey and Powell, 2011; Yakymchuk and Brown, 2014)。不同阶段生长的变质锆石具有不同的微量

元素特征,因为在封闭的体系中,锆石微量元素与锆石同时形成的矿物组合相关(吴元保等,2004)。在降温过程中生长的锆石,记录的变质年龄与峰期变质年龄的差异大小,与该岩石峰期之后的p-T轨迹有关(魏春景,2016)。如前所述,石榴夕线堇青石片麻岩中的锆石具有明显的核-边结构,核部多呈不规则状,具有振荡环带,显示碎屑锆石的特征,边部则具有显著的变质锆石特征,锆石边部数据点拟合出了一条很好的不一致线,上交点年龄为 $1\,133 \pm 4$ Ma(MSWD=1.18),应代表了该岩石的变质作用年龄。

独居石可以在进变质作用阶段生长(Johnson et al., 2015),在熔体冷却过程中结晶(Yakymchuk and Brown, 2014),在深熔作用过程中被分解(Yakymchuk, 2017)。因此,独居石可以对变质作用不同阶段进行记录。识别不同阶段的独居石,需结合独居石背散射图像、成分环带特征、微量元素特征和矿物包裹体(Williamms et al., 2007; Hetherington et al., 2017)。如前所述,石榴夕线堇青石片麻岩中的独居石颗粒具有核-边结构,核部多呈不规则,边部无明显内部结构或呈补丁状结构,13个边部数据点的 $^{207}\text{Pb}/^{206}\text{Pb}$ 加权平均年龄为 $1\,125 \pm 37$ Ma,该年龄应代表了该岩石的变质作用年龄。这与锆石获得变质年龄在误差范围内一致,本样品中无论是变质锆石还是独居石,均缺少对早古生代变质作用时代的记录。

相平衡模拟显示,石榴夕线堇青石片麻岩的峰期温压条件和p-T演化轨迹与相同地层单元且变质年龄为1.1 Ga的泥质片麻岩和石榴子石岩相平衡模拟结果相似(Wang et al., 2021b),虽然本文仅限制了峰期温压条件的下限,不能很好地限制其上限,但Wang等(2021b)限制泥质片麻岩和石榴子石岩的峰期温度可达840~900°C,表明该单元岩石普遍经历了1.1 Ga的高温变质作用。这表明该岩石要再次达到平衡,晚期构造热事件的温度条件应至少高于该峰期温度条件才足以改变或者抹掉该期的麻粒岩相变质作用记录(Wang et al., 2021b)。大致840~900°C的峰期温度与早古生代记录的麻粒岩相峰期温度范围(大致800~900°C)相一致(Li et al., 2019),这可能是1.1 Ga高温麻粒岩相变质作用得以保留的主要原因。Wang等(2021b)对石榴子石样品开展了独居石原位U-Pb定年,认为石榴子石岩中重结晶或新生长的1.1 Ga的独居石更像生长于进变质作用阶段。本研究显示石榴夕线堇青石片麻岩

峰期之后经历了略升温降压的 p - T 演化轨迹,如果变质锆石和独居石生长在熔体结晶过程中,该 1 133~1 125 Ma 的年龄也应近似代表了麻粒岩相峰期变质年龄。因此,本文研究的石榴夕线堇青石片麻岩的麻粒岩相变质作用应是对 1.1 Ga 的构造热事件的记录。

6.3 构造意义

乌兰北部中元古代晚期的构造热事件以 1.2~1.1 Ga 的花岗质侵入体、酸性火山岩和同时代的麻粒岩-角闪岩相变质岩为特征。前人已有一些初步的工作,得到变基性岩、眼球状花岗片麻岩、副片麻岩等的岩浆及变质年龄基本介于 1 135~1 104 Ma 之间(Yu et al., 2019; Wang et al., 2019, 2021a, 2021b; Xiao et al., 2020)。本项目组获得的眼球状花岗片麻岩的岩浆年龄为 1 172 Ma,察汗河岩群 c 岩组中的酸性火山岩夹层的时代为 1 139~1 136 Ma(未发表数据)。

Yu 等(2019)认为具有 $1\ 132 \pm 33$ Ma 的原岩岩浆结晶年龄的变质基性岩显示具有弧相关的地球化学特征,推测其形成于安第斯型弧的构造环境。Wang 等(2021b)根据原位独居石定年得到了副片麻岩约 1.11 Ga 的变质年龄,并根据泥质片麻岩中石榴子石+堇青石+夕线石+黑云母+斜长石+石英+钛铁矿及富石榴子石岩中尖晶石+石榴子石+黑云母+钛铁矿+夕线石的峰期矿物组合,计算得到更高的峰期变质温度(约 840~900°C)和更大范围的压力条件(0.7~1.1 GPa)。本研究获得石榴夕线堇青石片麻岩 1.1 Ga 的变质年龄和峰期温度约为 >790°C、压力 0.92~1.08 GPa 变质条件,并在峰期后经历了近等温降压的退变质作用。本项目组获得的 Mg-Al 麻粒岩的峰期条件为 920~940°C、0.54~0.57 GPa(未发表数据),表明中元古代晚期乌兰北部可能经历了超高温变质作用,该地区中元古代晚期的变质作用发生在高地温梯度的低压/高温条件下,结合区域地质概况,推断其可能形成于持续大洋俯冲作用下的弧或弧后构造环境。

1.2~0.9 Ga 是格林威尔造山事件的主要发生期,在全球范围内广泛分布,被认为是与 Rodinia 超大陆的形成有关(Li et al., 2008)。在中国中央造山带的前寒武纪陆块及造山带中(包括祁连、塔里木克拉通、柴达木地块、柴北缘 UHP 变质带、柴达木南缘等)广泛有 1.0~0.9 Ga 岩浆变质记录(陆松年等,

2002b; Gehrel et al., 2003; 董国安等, 2007; Ma et al., 2012; Song et al., 2012; Tung et al., 2013; Yu et al., 2013a; Wang et al., 2014; Huang et al., 2015; Zhang et al., 2017; Li et al., 2020; 耿元生等, 2020),多解释为与 Rodinia 超大陆聚合过程的陆-陆或弧-陆碰撞相关(Song et al., 2012; Tung et al., 2013; Yu et al., 2013a; Wang et al., 2014; Huang et al., 2015; Zhang et al., 2017),这一时代明显滞后于全球其他典型格林威尔期造山带。近年来,在中央造山带的西部及扬子地块西南缘等地陆续报道有 1.1~1.0 Ga 的岩浆及变质作用(Fu et al., 2019; Yu et al., 2019; Xiao et al., 2020; Teng et al., 2020; 何凡等, 2020; Wang et al., 2021a, 2021b; 张建新等, 2021; 毛小红等, 2021),多解释为与 Rodinia 超大陆汇聚过程中的俯冲或碰撞相关(Fu et al., 2019; Yu et al., 2019; Xiao et al., 2020; 何凡等, 2020; Wang et al., 2021a, 2021b)。由此可知,欧龙布鲁克地块及中国西部的各个前寒武纪块体均卷入了 1.1~0.9 Ga 的 Rodinia 超大陆汇聚过程。

此外,乌兰北部广泛分布 0.9 Ga 的花岗质岩石,前人和本项目组(未发表数据)的岩石地球化学研究显示这些花岗质岩石为弱过铝质-强过铝质 S 花岗岩特征(马建军等, 2018),具有碰撞造山花岗岩的特征。因此,结合区域地质资料,我们推测,从中元古代晚期(1.1 Ga)到新元古代早期(0.9 Ga),乌兰北部的岩浆-变质杂岩带经历了从俯冲增生到碰撞造山的演化过程,是全球 Rodinia 超大陆汇聚过程的响应。

7 结论

(1) 乌兰北部察汗河岩群的石榴夕线堇青石片麻岩经历了 1 133~1 125 Ma 的麻粒岩相变质作用,峰期温压条件为: $p = 0.92 \sim 1.08$ GPa 和 $t > 780^\circ\text{C}$,峰期之后经历了略升温降压的顺时针 p - T 演化轨迹。

(2) 乌兰北部察汗河岩群的石榴夕线堇青石片麻岩可能形成于持续大洋俯冲作用下的弧或弧后构造环境,乌兰北部的岩浆-变质杂岩带经历了从俯冲增生到碰撞造山的演化过程,是全球 Rodinia 超大陆汇聚过程的响应。

致谢 感谢两位审稿人对论文原稿提出了建设性的修改意见和建议,使作者受益匪浅。

References

- Andersen. 2002. Correction of common lead in U-Pb analyses that do not report ^{204}Pb [J]. *Chemical Geology*, 192 (1~2): 59~79.
- Bai Chundong, Zhuan Shaopeng, Mao Zhifang, et al. 2019. LA-ICP-MS Zircon U-Pb ages, geochemical characteristics and geotectonic significance of the metamorphosed volcanic rocks in Neoproterozoic Balongonggaer Formation in Tianjun County, Southern Qilian Mountain[J]. *Geological Review*, 65(3): 17(in Chinese with English abstract).
- Chen Nengsong, Wang Qinyan, Chen Qiang, et al. 2007. Components and metamorphism of the basements of the Qaidam and Oulongbuluke micro-continental blocks, and a tentative interpretation of paleocontinental evolution in NW-Central China[J]. *Earth Science Frontiers*, 14(1): 43~55 (in chinese with English abstract).
- Chen N S, Gong S L, Sun M, et al. 2009. Precambrian evolution of the Quanji Block, northeastern margin of Tibet: Insights from zircon U-Pb and Lu-Hf isotope compositions [J]. *Journal of Asian Earth Sciences*, 35 (3~4): 367~376.
- Chen N S, Zhang L, Sun M, et al. 2012. U-Pb and Hf isotopic compositions of detrital zircons from the paragneisses of the Quanji Massif, NW China: Implications for its early tectonic evolutionary history [J]. *Journal of Asian Earth Sciences*, 54: 110~130.
- Chen N S, Liao F X, Wang L, et al. 2013. Late Paleoproterozoic multiple metamorphic events in the Quanji Massif: Links with Tarim and North China Cratons and implications for assembly of the Columbia supercontinent [J]. *Precambrian Research*, 228: 102~116.
- Tung K A, Yang H J, Yang H Y, et al. 2007. SHRIMP U-Pb geochronology of the zircons from the Precambrian basement of the Qilian Block and its geological significances[J]. *Chinese Science Bulletin*, 52 (19): 2 687~2 701.
- Fu C L, Yan Z, Guo X Q, et al. 2019. Assembly and dispersal history of continental blocks within the Altun-Qilian-North Qaidam mountain belt, NW China [J]. *International Geology Review*, 61 (4): 424~447.
- Gehrels G E, Yin A and Wang X F. 2003. Detrital-zircon geochronology of the northeastern Tibetan plateau [J]. *Geological Society of America Bulletin*, 115 (7): 881~896.
- Geng Yuansheng, Kuang Hongwei, Du Lilin, et al. 2020. The characteristics of Meso-Neoproterozoic magmatic rocks in North China, South China and Tarim blocks and their significance of geological correlation[J]. *Acta Petrologica Sinica*, 36(8): 2 276~2 312(in Chinese with English abstract).
- Gong S L, Chen N S, Wang Q Y, et al. 2012. Early Paleoproterozoic magmatism in the Quanji Massif, northeastern margin of the Qinghai-Tibet Plateau and its tectonic significance: LA-ICPMS U-Pb zircon geochronology and geochemistry [J]. *Gondwana Research*, 21 (1): 152~166.
- He Fan and Song Shuguang. 2020. The Grenvillian-aged UHT granulite in Jinshukou region, East Kunlun Orogenic belt[J]. *Acta Petrologica Sinica*, 36(4): 1 030~1 040(in Chinese with English abstract).
- Hetherington C J, Backus E L, McFarlane C R M, et al. 2017. Origins of textural, compositional, and isotopic complexity in monazite and its petrochronological analysis[C]// Moser D E, Corfu F, Darling J R, et al. *Microstructural Geochronology. Planetary Records Down to Atom Scale*: American Geophysical Union Geophysical Monograph, 232: 63~90.
- Holland T and Powell R. 2003. Activity-composition relations for phases in petrological calculations: An asymmetric multicomponent formulation [J]. *Contributions to Mineralogy and Petrology*, 145(4): 492~501.
- Holland T J B and Powell R. 2011. An improved and extended internally consistent thermodynamic dataset for phases of petrological interest, involving a new equation of state for solids [J]. *Journal of Metamorphic Geology*, 29(3): 333~383.
- Hoskin P W O and Black L P. 2000. Metamorphic zircon formation by solid-state recrystallization of protolith igneous zircon [J]. *Journal of Metamorphic Geology*, 18 (4): 423~439.
- Huang H, Niu Y L, Nowell G, et al. 2015. The nature and history of the Qilian Block in the context of the development of the Greater Tibetan Plateau[J]. *Gondwana Research*, 28 (1): 209~224.
- Johnson T E, Clark C, Taylor R J M, et al. 2015. Prograde and retrograde growth of monazite in migmatites: An example from the Nagercoil Block, southern India [J]. *Geoscience Frontiers*, 6 (3): 373~387.
- Kelsey D E and Hand M. 2015. On ultrahigh temperature crustal metamorphism: Phase equilibria, trace element thermometry, bulk composition, heat sources, timescales and tectonic settings [J]. *Geoscience Frontiers*, 6 (3): 311~356.
- Kelsey D E and Powell L R. 2011. Progress in linking accessory mineral growth and breakdown to major mineral evolution in metamorphic rocks: A thermodynamic approach in the $\text{Na}_2\text{O}-\text{CaO}-\text{K}_2\text{O}-\text{FeO}-\text{MgO}-\text{Al}_2\text{O}_3-\text{SiO}_2-\text{H}_2\text{O}-\text{TiO}_2-\text{ZrO}_2$ system [J]. *Journal of Metamorphic Geology*, 29 (1): 151~166.
- Korhonen F J, Powell R and Stout J H. 2012. Stability of sapphirine+quartz in the oxidized rocks of the Wilson Lake Terrane, Labrador: Calculated equilibria in NCKFMASHTO [J]. *Journal of Metamorphic Geology*, 30(1): 21~36.
- Li X C, Niu M L, Yakymchuk C, et al. 2019. A paired metamorphic belt

- in a subduction-to-collision orogen: An example from the South Qilian-North Qaidam orogenic belt, NW China [J]. *Journal of Metamorphic Geology*, 37: 479~508.
- Li Xiucui, Niu Manlan, Yan Zhen, et al. 2015a. LP/HT metamorphic rocks in Wulan County, Qinghai Province: An Early Paleozoic paired metamorphic belt on the northern Qaidam Basin [J]. *Chinese Science Bulletin*, 60(35): 3 501~3 513 (in Chinese).
- Li Xiucui, Niu Manlan, Yan Zhen, et al. 2015b. SHRIMP zircon dating for migmatitic biotite plagioclase gneiss from Erlangdong Dakendaban Group in Wulan at the north margin of Qaidam Basin and its geological significance [J]. *Chinese Journal of Geology*, 50(3): 728~740 (in Chinese with English abstract).
- Li X W and Wei C J. 2016. Phase equilibria modelling and zircon age dating of pelitic granulites in Zhaojiayao, from the Jining Group of the Khondalite Belt, North China Craton [J]. *Journal of Metamorphic Geology*, 34(6): 595~615.
- Li Y L, Xiao W J, Li, Z Y, et al. 2020. Early Neoproterozoic magmatism in the Central Qilian block, NW China: Geochronological and petrogenetic constraints for Rodinia assembly [J]. *Geological Society of America Bulletin*, 132: 2 415~2 431.
- Li Z X, Bogdanova S V, Collins A S, et al. 2008. Assembly, configuration, and break-up history of Rodinia: a synthesis [J]. *Precambrian Research*, 160 (1~2): 179~210.
- Liao Fenxi, Gong Songlin, Dong Yanjun, et al. 2012. LA-ICP-MS zircon U-Pb age of meta-basic plutons in eastern Quanji massif: Evidence for Mesoproterozoic continental break-up [J]. *Geological Bulletin of China*, 31(8): 1 279~1 286 (in Chinese with English abstract).
- Liao F X, Zhang L, Chen N S, et al. 2014. Geochronology and geochemistry of meta-mafic dykes in the Quanji Massif, NW China: Paleo-proterozoic evolution of the Tarim Craton and implications for the assembly of the Columbia supercontinent [J]. *Precambrian Research*, 249: 33~56.
- Liao F X, Chen N S, Santosh M, et al. 2018. Paleoproterozoic Nb-enriched meta-gabbros in the Quanji Massif, NW China: Implications for assembly of the Columbia supercontinent [J]. *Geoscience Frontiers*, 9 (2): 577~590.
- Liu Y S, Hu Z C, Gao S, et al. 2008. In situ analysis of major and trace elements of anhydrous minerals by LA-ICP-MS without applying an internal standard [J]. *Chemical Geology*, 257 (1): 34~43.
- Liu Y S, Gao S, Hu Z C, et al. 2010. Continental and oceanic crust recycling-induced melt-peridotite interactions in the Trans-North China Orogen: U-Pb dating, Hf isotopes and trace elements in zircons from mantle xenoliths [J]. *Journal of Petrology*, 51 (1~2): 537~571.
- Lu Songnian, Wang Huichu, Li Huaikun, et al. 2002a. Redefinition of the “Dakendaban Group” on the northern margin of the Qaidam basin [J]. *Geological Bulletin of China*, 21(1): 19~23 (in Chinese with English abstract).
- Lu Songnian. 2002b. Preliminary Study of Precambrian Geology in the North Tibet-Qinghai Plateau [M]. Beijing: Geological Publishing House, 1~125 (in Chinese).
- Lu S N, Li H K, Zhang C L, et al. 2008. Geological and geochronological evidence for the Precambrian evolution of the Tarim Craton and surrounding continental fragments [J]. *Precambrian Research*, 160 (1~2): 94~107.
- Lu Zenglong, Zhang Jianxin, Mao Xiaohong, et al. 2020. Ordovician adakite-Nb-enriched basalt suite in the eastern North Qaidam Mountains: Implications for oceanic subduction and crustal accretion prior to deep continental subduction [J]. *Acta Petrologica Sinica*, 36 (10): 2 995~3 017 (in Chinese with English abstract).
- Lu Z L, Zhang J X and Mattinson C. 2018. Tectonic erosion related to continental subduction: An example from the eastern North Qaidam Mountains, NW China [J]. *Journal of Metamorphic Geology*, 36 (5): 653~666.
- Ludwig K R. 2003. User’s Manual for Isoplot 3.00: A Geochronological Toolkit for Microsoft Excel [M]. Berkeley, California: Berkeley Geochronology Center, California, Berkeley, 39.
- Ma Jianjun, Wang Heng, He Chuan, et al. 2018. Neoproterozoic post-collision magmatism in South Qilian Orogen, China: Evidenced by geochronology and geochemistry [J]. *Journal of Earth Sciences and Environment*, 40(2): 133~154 (in Chinese with English abstract).
- Ma X X, Shu L S, Santosh M, et al. 2012. Detrital zircon U-Pb geochronology and Hf isotope data from Central Tianshan suggesting a link with the Tarim Block: Implications on Proterozoic supercontinent history [J]. *Precambrian Research*, 206~207: 1~16.
- Mao Xiaohong, Zhang Jianxin, Lu Zenglong, et al. 2021. Early Paleozoic reactivation of the Precambrian basement on the northern margin of the Qilian block: Evidence from phase equilibria and zircon U-Pb dating of meta-mafic rocks [J]. *Acta Petrologica Sinica*, 37(10): 3 095~3 117 (in Chinese with English abstract).
- Mattinson C G, Wooden J L, Liou J G, et al. 2006. Age and duration of eclogite-facies metamorphism, North Qaidam HP/UHP terrane, Western China [J]. *Geochimica et Cosmochimica Acta*, 306 (9): 683~711.
- Mattinson C G, Menold C A, Zhang J X, et al. 2007. High- and ultra-high-pressure metamorphism in the North Qaidam and South Altyn Terranes, Western China [J]. *International Geology Review*, 49: 969~995.
- Niu Guangzhi, Huang Gang, Deng Changsheng, et al. 2016. LA-ICP-MS zircon U-Pb ages of metamorphic volcanic rocks in Bajonggongge’er Formation of South Qilian Mountain in Qinghai Province and their ge-

- ological significance [J]. *Geological Bulletin of China*, 35 (9): 1 441~1 447 (in Chinese with English abstract).
- Powell R and Holland T J B. 2008. On thermobarometry [J]. *Journal of Metamorphic Geology*, 26 (2): 155~179.
- Rubatto D, Williams I S and Buick I S. 2001. Zircon and monazite response to prograde metamorphism in the Reynolds Range, central Australia[J]. *Contributions to Mineralogy Petrology*, 140 (4): 458~468.
- Song S G, Niu Y L, Su L, et al. 2014. Continental orogenesis from ocean subduction, continent collision/subduction, to orogen collapse, and orogen recycling: The example of the North Qaidam UHPM belt, NW China [J]. *Earth-Science Review*, 129: 59~84.
- Song S G, Su L, Li X H, et al. 2010. Tracing the 850Ma continental flood basalts from a piece of subducted continental crust in the North Qaidam UHPM belt, NW China [J]. *Precambrian Research*, 183: 805~816.
- Song S G, Su L, Li X H, et al. 2012. Grenville-age orogenesis in the Qaidam-Qilian block: The link between South China and Tarim [J]. *Precambrian Research*, 220: 9~22.
- Song S G, Yang J S, Xu Z Q, et al. 2003. Metamorphic evolution of the coesite-bearing ultrahigh-pressure terrane in the North Qaidam, Northern Tibet, NW China [J]. *Journal of metamorphic Geology*, 21: 631~644.
- Song S G, Yang L M, Zhang Y Q, et al. 2017. Qi-Qin Accretionary belt in Central China Orogen: Accretion by trench jam of oceanic plateau and formation of intra-oceanic arc in the Early Paleozoic Qin-Qi-Kun Ocean [J]. *Science Bulletin*, 62 (15): 1 035~1 038.
- Song S G, Zhang L F, Niu Y L, et al. 2005. Geochronology of diamond-bearing zircons from garnet peridotite in the North Qaidam UHPM belt, Northern Tibetan Plateau: A record of complex histories from oceanic lithosphere subduction to continental collision [J]. *Earth and Planetary Science Letters*, 234: 99~118.
- Song S G, Zhang L F, Niu Y L, et al. 2006. Evolution from oceanic subduction to continental collision: A case study from the Northern Tibetan Plateau based on geochemical and geochronological data [J]. *Journal of Petrology*, 47: 435~455.
- Sun Jiaopeng, Chen Shiyue, Peng Yuan, et al. 2015. Determination of Early Cambrian zircon SHRIMP U-Pb datings in Zongwulong Tectonic Belt, northern margin of Qaidam Basin, and its geological significance [J]. *Geological Review*, 61 (4): 743~751 (in Chinese with English abstract).
- Teng X, Zhang J X, Mao X H, et al. 2020. The earliest Cambrian UHT metamorphism in the Qaidam block, western China: A record of the final assembly of Greater Gondwana? [J]. *Gondwana Research*, 87: 118~137.
- Tung K A, Yang H Y, Liu D Y, et al. 2013. The Neoproterozoic granitoids from the Qilian block, NW China: Evidence for a link between the Qilian and South China blocks [J]. *Precambrian Research*, 235: 163~189.
- Wang C, Wang Y H, Liu L, et al. 2014. The Paleoproterozoic magmatic-metamorphic events and cover sediments of the Tiekelik Belt and their tectonic implications for the southern margin of the Tarim Craton, northwestern China [J]. *Precambrian Research*, 254: 210~225.
- Wang C Y, Yu S Y, Sun D Y, et al. 2021a. Mesoproterozoic tectonic-thermal events in the Oulongbuluke Block, NW China: Constraints on the transition from supercontinent Columbia to Rodinia [J]. *Precambrian Research*, 352: 106010.
- Wang L, Johnston S T and Chen N S. 2019. New insights into the Precambrian tectonic evolution and continental affinity of the Qilian block: Evidence from geochronology and geochemistry of metasupracrustal rocks in the North Wulan terrane [J]. *Geological Society of America Bulletin*, 131 (9~10): 1 723~1 743.
- Wang L, Johnston S T, Chen N S, et al. 2021b. Late Mesoproterozoic low- p/T type metamorphism in the North Wulan terrane: Implications for the assembly of Rodinia [J]. *Geological Society of America Bulletin*, 133 (11~12): 2 243~2 265.
- Wang L, Wang H, He C, et al. 2016. Mesoproterozoic continental breakup in NW China: Evidence from gray gneisses from the North Wulan terrane [J]. *Precambrian Research*, 281: 521~536.
- Wang Qinyan, Chen Nengsong, Li Xiaoyan, et al. 2008. LA-ICPMS zircon U-Pb geochronological constraints on the tectonothermal evolution of the Early Paleoproterozoic Dakendaban Group in the Quanji Block, NW China [J]. *Chinese Science Bulletin*, 53 (14): 1 693~1 701 (in Chinese).
- Wang Q Y, Dong Y J, Pan Y M, et al. 2018. Early Paleozoic granulite-facies metamorphism and magmatism in the northern Wulan Terrane of the Quanji Massif: Implications for the evolution of the proto-Tethys Ocean in Northwestern China [J]. *Journal of Earth Science*, 29 (5): 1 081~1 101.
- Wei Chunjing. 2016. Granulite facies metamorphism and petrogenesis of granite (II): Quantitative modeling of the HT-UHT phase equilibria for metapelites and the petrogenesis of S-type granite [J]. *Acta Petropoligica Sinica*, 32 (6): 1 625~1 643 (in Chinese with English abstract).
- White R W and Powell R. 2002. Melt loss and the preservation of granulite facies mineral assemblages [J]. *Journal of Metamorphic Geology*, 20 (6): 621~832.
- White R W, Powell R and Clarke G L. 2002. The interpretation of reaction textures in Fe-rich metapelitic granulites of the Musgrave Block,

- central Australia: Constraints from mineral equilibria calculations in the system K_2O - FeO - MgO - Al_2O_3 - SiO_2 - H_2O - TiO_2 - Fe_2O_3 [J]. *Journal of Metamorphic Geology*, 20 (1): 41~55.
- White R W, Powell R, Holland T J B, et al. 2014. New mineral activity-composition relations for thermodynamic calculations in metapelitic systems [J]. *Journal of Metamorphic Geology*, 32(3): 261~286.
- Whitney D L and Evans B W. 2010. Abbreviations for names of rock-forming minerals [J]. *American Mineralogist*, 95: 185~187.
- Williams M L, Jercinovic M J and Hetherington C J. 2007. Microprobe monazite geochronology: Understanding geologic processes by integrating composition and chronology [J]. *Annual Review of Earth and Planetary Sciences*, 35: 137~175.
- Wu Y B and Zheng Y F. 2004. Genesis of zircon and its constraints on interpretation of U-Pb age [J]. *Chinese Science Bulletin*, 49 (15): 1 554~1 569.
- Xiang H and Connolly J A D. 2022. GeoPS: An interactive visual computing tool for thermodynamic modelling of phase equilibria [J]. *Journal of Metamorphic Geology*, 40(2): 243~255.
- Xiao Q H, Lu X X, Wang F, et al. 2004. Age of Yingfeng rapakivi granite pluton on the north flank of Qaidam and its geological significance [J]. *Science in China (Series D)*, 47(4): 357~365.
- Xiao Z X, Ma L C, Jiang W, et al. 2020. Grenville-age orogenic event along the northeastern margin of the Quanji massif, NW China: Constraints from ~1.1 Ga migmatite [J]. *Geosciences Journal*, 24: 1~18.
- Yakymchuk C and Brown M. 2014. Behaviour of zircon and monazite during crustal melting [J]. *Journal of the Geological Society*, 171(4): 465~479.
- Yakymchuk C. 2017. Behaviour of apatite during partial melting of metapelites and consequences for prograde suprasolidus monazite growth [J]. *Lithos*, 274~275: 412~426.
- Yan Z, Fu C L, Aitchison J C, et al. 2019. Early Cambrian Muli arc-ophiolite complex: A relic of the Proto-Tethys oceanic lithosphere in the Qilian Orogen, NW China [J]. *International Journal of Earth Sciences*, 108(4): 1 147~1 164.
- Yang Jingsui, Xu Zhiqin, Li Haibing, et al. 1998. The eclogites have been found in the northern Qaidam Basin, western China [J]. *Science in Bulletin*, 43(14): 1 544~1 549 (in Chinese).
- Yu S Y, Zhang J X, Del Real P G, et al. 2013a. The Grenvillian orogeny in the Altun-Qilian-North Qaidam mountain belts of northern Tibet Plateau: Constraints from geochemical and zircon U-Pb age and Hf isotopic study of magmatic rocks [J]. *Journal of Asian Earth Sciences*, 73: 372~395.
- Yu S Y, Zhang J X, Li H K, et al. 2013b. Geochemistry, zircon U-Pb geochronology and Lu-Hf isotopic composition of eclogites and their host gneisses in the Dulan area, North Qaidam UHP terrane: New evidence for deep continental subduction [J]. *Gondwana Research*, 23: 901~919.
- Yu Shengyao, Zhang Jianxin, Sun Deyou, et al. 2014. Partial melting of subducted continental plate during exhumation from the North Qaidam UHP terrane, western China [J]. *Acta Petrologica Sinica*, 30 (8): 2287~2296 (in Chinese with English abstract).
- Yu S Y, Li S Z, Zhang J X, et al. 2019. Grenvillian orogeny in the Oulongbuluke Block, NW China: Constraints from an ~1.1 Ga Andean-type arc magmatism and metamorphism [J]. *Precambrian Research*, 320: 424~437.
- Zhang C, Bader T, Zhang L F, et al. 2017. The multi-stage tectonic evolution of the Xitieshan terrane, North Qaidam orogen, western China: From Grenville-age orogeny to early-Paleozoic ultrahigh-pressure metamorphism [J]. *Gondwana Research*, 41: 290~300.
- Zhang G B, Song S G, Zhang L F, et al. 2008. The subducted oceanic crust within continental-type UHP metamorphic belt in the North Qaidam, NW China: Evidence from petrology, geochemistry and geochronology [J]. *Lithos*, 104: 99~118.
- Zhang G B, Zhang L F, Song S G, et al. 2009. UHP metamorphic evolution and SHRIMP geochronology of a coesite-bearing meta-ophiolitic gabbro in the North Qaidam, NW China [J]. *Journal of Asian Earth Sciences*, 35: 310~322.
- Zhang Jianxin, Lu Zenglong, Mao Xiaohong, et al. 2021. Revisiting the Precambrian micro-continental blocks within the Early Paleozoic orogenic system of the northeastern Qinghai-Tibet Plateau: Insight into the origin of Proto-Tethyan Ocean [J]. *Acta Petrologica Sinica*, 37 (1): 74~94 (in Chinese with English abstract).
- Zhang J X, Mattinson C G, Yu S Y, et al. 2010. U-Pb zircon geochronology of coesite-bearing eclogites from the southern Dulan area of the North Qaidam UHP terrane, northwestern China: Spatially and temporally extensive UHP metamorphism during continental subduction [J]. *Journal of metamorphic Geology*, 28: 955~978.
- Zhang J X, Meng F C, Li J P, et al. 2009a. Coesite in eclogite from the North Qaidam Mountains and its implications [J]. *Chinese Science Bulletin*, 54: 618~623.
- Zhang Jianxin, Meng Fancong and Mattinson C G. 2007. Progress, controversies and challenge of studies on South Altyn Tagh-North Qaidam HP/UHP metamorphic belt [J]. *Geological Journal of China Universities*, 13(3): 526~545 (in Chinese with English abstract).
- Zhang J X, Meng F C and Yang J S. 2004. Eclogitic metapelites in the western segment of the North Qaidam Mountains: Evidence on “in situ” relationship between eclogite and its country rock [J]. *Science in China (Series D)*, 47(12): 1 102~1 112.
- Zhang J X, Yu S Y, Mattinson C G. 2017. Early Paleozoic polyphase

- metamorphism in northern Tibet, China [J]. *Gondwana Research*, 41: 267~289.
- Zhang Jianxin, Yu Shengyao, Meng Fancong, et al. 2009b. Paired high-pressure granulite and eclogite in collision orogens and their geodynamic implications [J]. *Acta Petrologica Sinica*, 25(9): 2 050~2 066 (in chinese with English abstract).
- Zhang Shuai, Wang Chao, Hao Jiangbo, et al. 2022. U-Pb geochronology, provenance and geological implications of Early Paleozoic volcano-sedimentary rocks in the Danghenanshan-Muli area, Central Qilian belt [J]. *Acta Petrologica Sinica*, 38(3): 813~829 (in chinese with English abstract).

附中文参考文献

- 白春东, 专少鹏, 毛志芳, 等. 2019. 南祁连天峻巴龙贡嘎尔组变质火山岩 LA-ICP-MS 锆石 U-Pb 年龄、地球化学特征及构造意义 [J]. 地质论评, 65(3): 17.
- 陈能松, 王勤燕, 陈 强, 等. 2007. 柴达木和欧龙布鲁克陆块基底的组成和变质作用及中国中西部古大陆演化关系初探 [J]. 地学前缘, 14: 43~55.
- 董国安, 杨怀仁, 杨宏仪, 等. 2007. 祁连地块前寒武纪基底锆石 SHRIMP U-Pb 年代学及其地质意义 [J]. 科学通报, 52(13): 1 572~1 585.
- 耿元生, 旷红伟, 杜利林, 等. 2020. 华北, 华南, 塔里木三大陆块中-新元古代岩浆岩的特征及其地质对比意义 [J]. 岩石学报, 36(8): 2 276~2 312.
- 何 凡, 宋述光. 2020. 东昆仑金水口地区格林威尔期超高温麻粒岩 [J]. 岩石学报, 36(4): 1 030~1 040.
- 李秀财, 牛漫兰, 同 璇, 等. 2015a. 青海省乌兰县早古生代低压高温变质岩:柴北缘存在双变质带? [J]. 科学通报, 60(35): 3 501~3 513.
- 李秀财, 牛漫兰, 同 璇, 等. 2015b. 柴北缘乌兰县二郎洞达肯大坂岩群中混合岩化黑云斜长片麻岩锆石 SHRIMP 测年及其意义 [J]. 地质科学, 50(3): 728~740.
- 廖梵汐, 龚松林, 董彦君, 等. 2012. 柴达木盆地北缘全吉地块东端变基性岩体 LA-ICP-MS 锆石 U-Pb 年龄:中元古代陆块裂解的证据 [J]. 地质通报, 31(8): 1 279~1 286.
- 陆松年. 2002. 青藏高原北部前寒武纪地质初探 [M]. 地质出版社.
- 陆松年, 王惠初, 李怀坤, 等. 2002. 柴达木盆地北缘达肯大坂群的再厘定 [J]. 地质通报, 21(1): 19~23.
- 路增龙, 张建新, 毛小红, 等. 2020. 柴北缘东段奥陶纪埃达克岩-富 Nb 玄武岩:对大陆深俯冲之前大洋俯冲及地壳增生的启示 [J]. 岩石学报, 36(10): 2 995~3 017.
- 马建军, 王 琦, 何 川, 等. 2018. 南祁连造山带新元古代后碰撞岩浆作用:年代学和地球化学证据 [J]. 地球科学与环境学报, 40(2): 133~154.
- 毛小红, 张建新, 路增龙, 等. 2021. 祁连地块北缘前寒武基底早古生代再活化:变基性岩相平衡模拟和锆石年代学证据 [J]. 岩石学报, 37(10): 3 095~3 117.
- 牛广智, 皇岗, 邓昌生, 等. 2016. 青海南祁连巴龙贡嘎尔组变火山岩 LA-ICP-MS 锆石 U-Pb 年龄及其地质意义 [J]. 地质通报, 35(9): 1 441~1 447.
- 青海省地质矿产局. 1991. 青海省区域地质志 [M]. 北京: 地质出版社, 1~622.
- 孙娇鹏, 陈世悦, 彭 渊, 等. 2015. 柴达木盆地北缘宗务隆构造带早古生代锆石 SHRIMP 年龄的测定及其地质意义 [J]. 地质论评, 61(4): 743~751.
- 王勤燕, 陈能松, 李晓彦, 等. 2008. 全吉地块基底达肯大坂岩群和热事件的 LA-ICP-MS 锆石 U-Pb 定年 [J]. 科学通报, 53(14): 1 693~1 701.
- 魏春景. 2016. 麻粒岩相变质作用与花岗岩成因 II: 变质泥质岩高温-超高温变质相平衡与 S 型花岗岩成因的定量模拟 [J]. 岩石学报, 32: 1 625~1 643.
- 吴元保, 郑永飞. 2004. 锆石成因矿物学研究及其对 U-Pb 年龄解释的制约 [J]. 科学通报, 49: 1 589~1 604.
- 肖庆辉, 卢欣祥, 王菲, 等. 2003. 柴达木北缘鹰峰环斑花岗岩的时代及地质意义 [J]. 中国科学(D辑:地球科学), 33(12): 1 193~1 200.
- 杨经绥, 许志琴, 李海兵, 等. 1998. 我国西部柴北缘地区发现榴辉岩 [J]. 科学通报, 43: 1 544~1 549.
- 于胜尧, 张建新, 孙德有, 等. 2014. 柴北缘大陆深俯冲板片折返过程中的深熔作用研究 [J]. 岩石学报, 30(8): 2 287~2 296.
- 张建新, 路增龙, 毛小红, 等. 2021. 青藏高原东北缘早古生代造山系中前寒武纪微陆块的再认识——兼谈原特提斯洋的起源 [J]. 岩石学报, 37(1): 74~94.
- 张建新, 孟繁聪, 李金平, 等. 2009a. 柴达木北缘榴辉岩中的柯石英及其意义 [J]. 科学通报, 54: 618~623.
- 张建新, 孟繁聪, Mattinson C G. 2007. 南阿尔金-柴北缘高压-超高压变质带研究进展、问题及挑战. 高校地质学报 [J], 13(3): 526~545.
- 张建新, 孟繁聪, 杨经绥. 2004. 柴北缘西段榴辉岩相的变质泥质岩——榴辉岩与围岩原地关系的证据 [J]. 中国科学(D辑:地球科学), 34: 825~834.
- 张建新, 于胜尧, 孟繁聪, 等. 2009b. 造山带中成对出现的高压麻粒岩与榴辉岩及其地球动力学意义 [J]. 岩石学报, 25(9): 2 050~2 066.
- 张 帅, 王 超, 郝江波, 等. 2022. 中祁连党河南山-木里地区早古生代火山-沉积岩系锆石 U-Pb 年代学、物源示踪及其地质意义 [J]. 岩石学报, 38(3): 813~829.